

Learning and Evaluating Hierarchical Feature Representations

Depanshu Sani Saket Anand
Indraprastha Institute of Information Technology, Delhi, India

<https://sites.google.com/iiitd.ac.in/hier-cos>

Abstract

Hierarchy-aware representations ensure that the semantically closer classes are mapped closer in the feature space, thereby reducing the severity of mistakes while enabling consistent coarse-level class predictions. Towards this end, we propose a novel framework, Hierarchical Composition of Orthogonal Subspaces (Hier-COS), which learns to map deep feature embeddings into a vector space that is, by design, consistent with the structure of a given taxonomy tree. Our approach augments neural network backbones with a simple transformation module that maps learned discriminative features to subspaces defined using a fixed orthogonal frame. This construction naturally improves the severity of mistakes and promotes hierarchical consistency. Furthermore, we highlight the fundamental limitations of existing hierarchical evaluation metrics popularly used by the vision community and introduce a preference-based metric, Hierarchically Ordered Preference Score (HOPS), to overcome these limitations. We benchmark our method on multiple large and challenging datasets having deep label hierarchies (ranging from 3 – 12 levels) and compare with several baselines and SOTA. Through extensive experiments, we demonstrate that Hier-COS achieves state-of-the-art hierarchical performance across all the datasets while simultaneously beating top-1 accuracy in all but one case. We also demonstrate the performance of a Vision Transformer (ViT) backbone and show that learning a transformation module alone can map the learned features from a pre-trained ViT to Hier-COS and yield substantial performance benefits.

1. Introduction

Advanced machine learning techniques powered by deep neural networks have demonstrated remarkable scalability in classification tasks, successfully handling thousands or even millions of classes [1, 32]. This success highlights the capability of neural networks to learn highly discriminative feature representations. However, most of these algorithms operate under the assumption that all negative classes are equally unrelated to the target class, effectively treating

each class independently. In reality, classes often exhibit semantic relationships, which are typically structured and far from independent [2, 17, 28, 31, 35]. This oversimplification can lead to feature representations where errors are arbitrary and unstructured. Semantic knowledge, such as hierarchies that express relationships like *is-a*, *part-of* or *type-of* [24, 32, 35], is often available but remains underutilized. By ignoring these inter-class relationships, despite showing impressive performance, these algorithms can drastically fail when they make mistakes, which makes them especially risky in safety-critical applications.

Incorporating hierarchy-aware feature representations offers a significant advantage by structuring the feature space based on semantic relationships. This property has been extensively studied [3, 5, 6, 10, 11, 20, 36] and applied to mitigate failures in safety-critical systems. Such representations ensure that classes with greater semantic similarity are closer in the feature space, enabling more meaningful predictions even in the event of errors.

For instance, in the context of an object recognition model for an autonomous vehicle, a *cyclist* and a *pedestrian* are highly correlated as both are vulnerable road users; hence, we may *prefer* to misclassify a *cyclist* as a *pedestrian* rather than a *car* or a *truck*. Moreover, these representations intrinsically allow the inference of the coarse-level class labels. Therefore, a strong hierarchy-aware feature representation should ideally (i) reduce the severity of mistakes, and (ii) predict consistent hierarchical class labels, i.e., the predicted class labels at all coarser levels should be ancestors of the predicted leaf class.

To quantify the consistency of hierarchical predictions, Full Path Accuracy (FPA) [27] can be used that measures the proportion of samples correctly classified at all hierarchical levels. Meanwhile, the severity of mistakes can be evaluated using height of the tree rooted at the Lowest Common Ancestor (LCA) between predicted and true classes [5, 16]. As pointed out by [11], we also observe that the averaging of LCA obfuscates the nuances resulting from different structures of hierarchy trees, making the resulting metrics like Mistake Severity (MS) [5] and Average Hierarchical Distance (AHD) [16] difficult to interpret. Moreover,

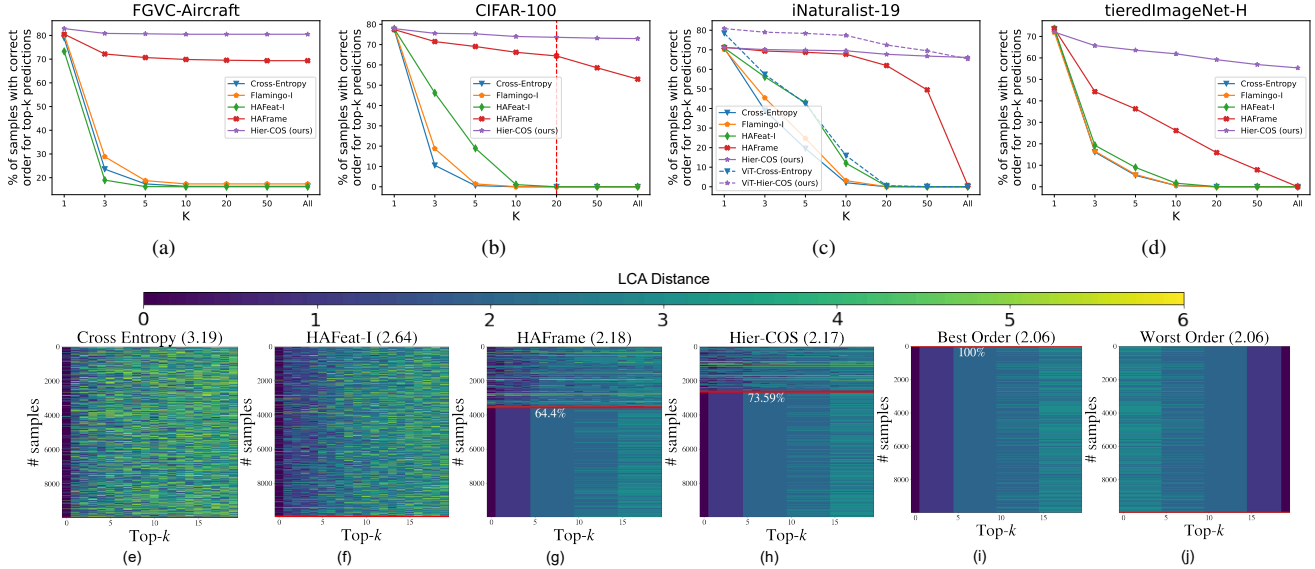


Figure 1. Several hierarchical classification methods report performance metrics like MS and AHD@ k paired with top-1 or top- k accuracies. While top- k predictions are rank-ordered, metrics like AHD@ k are *permutation invariant*, making them inadequate at capturing the true hierarchical classification performance. By comparing the rank order of the top- k predictions with their *LCA-based* ground truth order, we highlight that the evaluation metrics are inadequate and recent hierarchical classification models insufficiently capture the hierarchy structure. Subfigures (a)—(d) show that the percentage of samples with a correct prediction order decreases significantly as k increases across four hierarchical datasets, especially for complex datasets with deep hierarchies. This trend is also evident for transformer-based architectures, as shown in (c). In (e)—(h), we compare the LCA distances between ground truths and the top-20 predictions for all the test samples from CIFAR-100 (analogous to $k = 20$ in (b); red line). The AHD@20 metric is reported in parentheses next to the corresponding method name. The percentage of samples having the correct ordering (i.e., same predicted ordering as the ground truth) is nearly zero for (e) and (f) and is substantially higher ($\sim 64.4\%$) for (g) and even higher ($\sim 73.5\%$) for the proposed method (h). However, we see that the AHD@20 improves substantially from (e) to (f), moderately from (f) to (g) and marginally from (g) to (h). This is characteristic of using averaging, i.e., a *permutation invariant* aggregation of the LCA distance in AHD@ k and similar metrics. This limitation gets much worse in (i) which shows the perfect ordering for all samples with a 100% top-1 accuracy and an AHD@20 score of 2.06. In (j), we simply reverse the perfect order for each sample to get 0% top-1 accuracy, but the AHD@20 score remains the same at 2.06. The absolute value of AHD@ k depends on the properties of the hierarchy tree (skewness, branching factor and height), thus limiting its interpretability.

these metrics often are not sufficient on their own and need to be paired with the top-1 accuracy. Despite these limitations, the idea of the severity of mistakes emphasizes that not all misclassifications are equal; instead, there exists a preferred ordering of the set of incorrect classes based on the LCA distances within the label hierarchy.

The existing methods for hierarchical classification are trained using specially designed label embeddings [3, 5, 21], loss functions [5, 7, 34] and/or architectures [6, 11, 20, 36] that reduce the severity of mistakes. Methods trained with separate classifiers for each hierarchical level [6, 20] also impose additional constraints to promote hierarchical consistency. Fig. 1 highlights the limitations of various hierarchical classification methods and evaluation metrics. In this paper, we build upon the observation that deep learning based classifiers already excel at learning discriminative features but can drastically fail when they make mistakes, thereby proposing a framework for constructing a *vector space*, $V_{\mathcal{T}}$, that is inherently aware of — and implicitly con-

sistent with — the given hierarchy tree \mathcal{T} . Specifically, we show that neural networks can be augmented with a simple transformation module to enable mapping of the discriminative features, extracted from a neural network backbone, to $V_{\mathcal{T}}$; naturally improving the severity of mistakes and promoting hierarchical consistency. We further highlight some of the key limitations of commonly used hierarchical evaluation metrics and propose a preference-based evaluation metric for benchmarking hierarchy-aware classifiers. We summarize our contributions below

1. We present Hierarchical Composition of Orthogonal Subspaces (Hier-COS), a novel framework to map features extracted from a deep learning backbone to a vector space that is, by design, consistent with a given label hierarchy tree. We demonstrate that a simple transformation module can learn this mapping, leading to a significant reduction in the severity of mistakes and improvement in consistent prediction of hierarchical class labels.

2. We highlight crucial shortcomings in evaluation metrics popularly used to evaluate hierarchical classification models in the vision community [5, 15, 16]. We review the standard metrics used in information retrieval and ranking systems literature while highlighting the drawbacks of extending them to hierarchical classification [13, 14, 33]. We address these limitations and present a novel metric, Hierarchically Ordered Preference Score (HOPS), based on preference ordering [9].
3. We evaluate our method on four hierarchical datasets: FGVC-Aircraft (3 levels) [23], CIFAR-100 (5 levels) [17], iNaturalist-19 (7 levels) [35] and tieredImageNet (12 levels) [31]. We achieve state-of-the-art (SOTA) on three datasets and competitive performance on tieredImageNet-H.

2. Related Work

Learning representations that capture the semantic hierarchy has been shown to directly correlate with making better mistakes [5, 11] and robustness [12]. In recent years, several works have exploited the taxonomy, not only for standard classification tasks [6, 10] but also for image retrieval [3, 29], open set recognition [4, 8, 19] and neural collapse [20]. Label embedding methods map ground truth class labels to vector spaces where their relative locations represent semantic relationships and maximize the similarity between the feature vector and fixed label embeddings [3, 5, 10, 21, 25]. Hierarchical-loss methods incorporate hierarchical information directly into the loss function [5, 7, 34]. Hierarchical-architecture methods, discussed in more detail in this section, modify the classifier architecture to leverage the label hierarchy structure.

Wu et al. [36] developed a multi-task loss function where independent classification heads are used for classes at different granularity, i.e., levels of the label hierarchy. All the classifiers share a joint feature extractor and the cross-entropy losses of all levels are optimized jointly. Similarly, Chang et al. [6] also propose to train additional classifiers for each level of granularity, although while disentangling the feature vectors for each level of granularity. This allows the learning of coarse and fine-grained features; however, it is limited to small hierarchies because of explicit partitioning of the feature space. To mitigate this, Garg et al. [11] utilize the shared feature extractor and use a cross-entropy loss at the finest level and aim to achieve hierarchical consistency by introducing a soft hierarchical consistency, geometric consistency and margin loss.

All these methods rely on training an additional classifiers, often one at each level paired with additional loss terms, making them harder to train, more resource-intensive, and more difficult to scale to larger hierarchies. Moreover, with independent classifiers, additional constraints are needed to maintain hierarchical consistency.

More recently, Liang et al. [20] propose to learn a transformation module to a fixed hierarchy-aware frame that defines a single classifier. They leverage the concept of neural collapse [26] that suggests that the within-class means of all classes and their respective classifier weights tend to collapse to the vertices of a simplex Equiangular Tight Frame (ETF). The authors propose a Hierarchy-Aware Frame (HAFrame) for hierarchical classification wherein, unlike an ETF, the angular separation between classes is not equal and semantically closer classes have a smaller angular separation. Unlike previous methods, instead of using a trainable output layer they propose to fix the classifier weights to a fixed HAFrame. They propose additional transformation layers that are learned to map the features onto the HAFrame. They use a simple cross-entropy loss and pair-wise cosine similarity loss between the fixed frame and penultimate features. Despite improving accuracy and hierarchical performance, HAFrame does not adequately capture the label hierarchy structure, as shown in Fig. 1.

In this work, we propose a novel framework for hierarchy-aware feature representations that naturally improve the severity of mistakes and inherently promotes hierarchical consistency for any backbone network. Specifically, our proposed framework (i) uses a subspace approach to define a hierarchical structure similar to [22, Def. 2] (ii) leverages orthogonality constraints for generalization-specialization relations [37, Sec. 1], and (iii) learns a function to map features onto a fixed frame, similar to [20].

3. Constructing Hierarchy-aware Subspaces

Deep learning-based recognition methods typically assume that feature vectors align with the direction of their corresponding classification weight vectors. In contrast, we propose that feature vectors can reside within the span of the weight vectors rather than being strictly aligned. Therefore, unlike an ETF, where the pairwise angular separation $\cos^{-1}\left(-\frac{1}{K-1}\right)$ between the weight vectors tends to be orthogonal as the number of classes (K) increases [26], the maximum angular separation between subspaces is independent of K and is always orthogonal. Based on this observation, we enforce classifier weight vectors to be orthogonal. This implies that all the leaf classes would live in disjoint and orthogonal subspaces. However, this formulation is unaware of the semantic relationships between the leaf classes. To address this, we emphasize that any super-class can be interpreted as a vector space composed of the subspaces corresponding to all its children. For instance, the vector space spanned by the weight vectors corresponding to `car` and `truck` belongs to the super-class `vehicle`¹. But if the weight vectors corresponding to the leaf classes are orthogonal, the hierarchical composition of

¹See Fig. 8 in the supplementary for a conceptual illustration.

subspaces would still enforce the leaf classes to be orthogonal because each subspace only spans one dimension i.e., the corresponding weight vector. Therefore, we propose that the dimensionality of these subspaces should increase such that the number of common dimensions between them is directly proportional to the number of their common ancestors. We now formally define our Hierarchical Composition of Orthogonal Subspaces (Hier-COS) framework.

3.1. Problem Setup and Notation

We consider a dataset \mathcal{X} and a set of class labels \mathcal{Y} . We are given the semantic relationship between the classes \mathcal{Y} in the form of a hierarchy tree \mathcal{T} comprising of the set of nodes, $\mathcal{V}_{\mathcal{T}} = \{v_1, \dots, v_n\} \cup \{v_0\}$, where v_0 denotes the root node representing the universal class and is never used. The tree \mathcal{T} has height H with the number of nodes at each level given by $\{K_1, \dots, K_H\}$. We separately define the set of K leaf nodes as $\mathcal{V}_{\ell} = \{v_{y_1}, \dots, v_{y_K}\} \subset \mathcal{V}_{\mathcal{T}}$ to accommodate for leaf nodes at any height, a property often observed in naturally occurring label hierarchies. Here, the indices y_1, \dots, y_K are the fine-grained class labels \mathcal{Y} . For each node $v_i \in \mathcal{V}_{\mathcal{T}}$, we define the set of its ancestors (excluding v_0) as $f_a(v_i)$ and the set of its descendants as $f_d(v_i)$.

In order to construct a vector space composed of orthogonal subspaces, we choose an arbitrary and fixed orthonormal basis $\mathcal{E} = \{e_1, e_2, \dots, e_n\}$ of \mathbb{R}^n . Without loss of generality, we create an arbitrary bijective assignment of basis vectors $e_i \in \mathcal{E}$ to nodes $v_i \in \mathcal{V}_{\mathcal{T}}$. We define $\mathcal{E}^{(l)}$ as the set of basis vectors corresponding to the nodes at level l . For a given node $v_i \in \mathcal{V}_{\mathcal{T}}$, we also define \mathcal{E}_i^a as the basis set corresponding to $f_a(v_i)$ and \mathcal{E}_i^d as the set of basis corresponding to $f_d(v_i)$. For defining the vector space corresponding to a node v_i , we define the basis set as $\mathcal{E}_i = \mathcal{E}_i^a \cup e_i \cup \mathcal{E}_i^d$, and the corresponding subspace as $V_i = \text{span}(\mathcal{E}_i), \forall i \in [n]$, where $[n] = \{k \mid k \in \mathbb{Z}^+, k \leq n\}$ and $V_{\mathcal{T}} = \text{span}(\mathcal{E})^2$.

Characteristics of Hier-COS: Based on this construction, it is easy to see that any leaf node $v_{y_i} \in \mathcal{V}_{\ell}$ corresponds to a subspace spanned by the basis vectors corresponding to this leaf node and all of its ancestors. With the increase in the number of common ancestors between any two leaf nodes, the overlap of the subspaces also increases, and so does the similarity between the leaf classes. When a non-leaf node $v_i \in \{\mathcal{V}_{\mathcal{T}} \setminus \mathcal{V}_{\ell}\}$ is a super-class at a certain height h of the tree and has a corresponding subspace spanned by the basis vectors of its ancestors, itself and all of its descendants. Hence, by design, Hier-COS allocates higher dimensions to subspaces of classes with more ascendants and descendants. This is a desirable property as we expect larger subspaces to accommodate more complex intra-class variations at coarser granularity and yet retain discriminative features at finer levels³.

²A summary of notations is given in Table 8 in the supplementary.

³See Section 11 in the supplementary for a more detailed discussion.

3.2. Learning Problem Formulation

Using the Hier-COS framework, we compose the vector space $V_{\mathcal{T}}$ such that $V_i \subset V_{\mathcal{T}}, i = [n]$. In order to learn hierarchical representations consistent with \mathcal{T} , we begin with a backbone feature extractor $f_{\Theta} : \mathcal{X} \rightarrow Z \subseteq \mathbb{R}^d$ that has sufficient capacity to perform flat classification over the label set \mathcal{Y} . Our goal is to use this feature extractor as a backbone and learn a mapping $f_{\theta} : Z \rightarrow V_{\mathcal{T}}$ from the feature space Z to a vector space $V_{\mathcal{T}} = \mathbb{R}^n$, i.e., $\mathbf{x} = [x_1, \dots, x_n]^{\top} = f_{\theta}(\mathbf{z}), \mathbf{z} \in Z$. Note that the orthonormal vectors $e_i \in \mathcal{E}$ serve as canonical basis for $\mathbf{x} \in V_{\mathcal{T}}$, i.e., $|x_i|, i \in [n]$ are the components along the basis vector e_i .

Based on this construction, we define the distance between a point and the subspace using orthogonal projections. Consider a vector $\mathbf{x} \in V_{\mathcal{T}}$ and a subspace $V_{y_j} \subset V_{\mathcal{T}}$. The squared distance between \mathbf{x} and V_{y_j} is computed as the distance between the point \mathbf{x} and its orthogonal projection onto V_{y_j} , computed using the projection operator $\mathbb{P}_{\mathcal{E}_{y_j}}$, i.e.,

$$d_S^2(\mathbf{x}, V_{y_j}) = \|\mathbb{P}_{\neg\mathcal{E}_{y_j}} \mathbf{x}\|^2 = \|\mathbf{x}_{V_{y_j}^{\perp}}\|^2 = \sum_{e \in \neg\mathcal{E}_{y_j}} x_e^2 \quad (1)$$

where, $\|\cdot\|$ is the L-2 norm operator, and with a slight abuse of notation, we define $\neg\mathcal{E}_{y_j} := \{\mathcal{E} \setminus \mathcal{E}_{y_j}\}$ that serves as the set of basis vectors corresponding to the orthogonal complement of V_{y_j} , i.e., $V_{y_j}^{\perp}$. We also define $\mathbf{x}_{V_{y_j}}$ and $\mathbf{x}_{V_{y_j}^{\perp}}$ as projections of \mathbf{x} onto V_{y_j} and $V_{y_j}^{\perp}$, respectively, such that $\mathbf{x} = \mathbf{x}_{V_{y_j}} + \mathbf{x}_{V_{y_j}^{\perp}}$. Now, consider a vector \mathbf{x} that corresponds to an *ideal sample* from class y_i , such that $\mathbf{x} \in V_{y_i}$, i.e., $\|\mathbf{x}_{V_{y_i}^{\perp}}\| = 0$. If the leaf classes y_i and y_j have a common parent, i.e., $LCA(y_i, y_j) = 1$, from equation (1), it is easy to see that the distance $d_S(\mathbf{x}, V_{y_j}) = |x_{e_{y_i}}|$ because $|x_e| = 0 \forall e \in \{\neg\mathcal{E}_{y_j} \setminus e_{y_i}\}$. Generalizing this idea to an arbitrary class y_k , the distance $d_S(\mathbf{x}, V_{y_k})$ for any $\mathbf{x} \in V_{y_i}$ is dependent only the components $|x_e|, e \in \{\mathcal{E}_{y_i} \setminus \mathcal{E}_{y_k}\}$. If the projection norm of the feature vector is concentrated entirely on the leaf, i.e. $|x_e| = 0, \forall e \in \{\mathcal{E} \setminus e_{y_i}\}$, the distance between all the classes would be equal, i.e. $|x_{e_{y_i}}|$, defaulting to *flat* classification. Contrarily, if the projection norm is concentrated entirely on the ancestors ($\mathcal{E}_{y_i}^a$) and $|x_{e_{y_i}}| = 0$, the leaf classes will be inseparable. Accordingly, we propose to distribute the magnitude of \mathbf{x} across the basis $e \in \mathcal{E}_{y_i}$ to promote high leaf-level discrimination while respecting the semantic similarity via coarser classes. Therefore, we use a monotonically decreasing weight function to distribute the magnitude of \mathbf{x} as we move from the basis vectors of the leaf node to the root. Furthermore, we desire $|x_e| = 0, \forall e \in \neg\mathcal{E}_{y_i}$, resulting in a sparse vector \mathbf{x} .

We expect this design of $V_{\mathcal{T}}$ paired with the powerful backbone networks to have a modest demand on the mapping function f_{θ} and on the loss function. We simply reuse the transformation module proposed in HAFrame [20] to

construct f_θ , which is augmented to the backbone network to train end-to-end using the loss function below.

3.3. Loss Function

Given a feature vector $\mathbf{x} = [x_1, \dots, x_n]^\top \in V_{\mathcal{T}}$, our objective is to learn the distribution of $|x_i| \forall i \in [n]$. It is worth noting that we do not assume all the leaf nodes to be at the same level, thereby denoting the level of a leaf node as $h \leq H$. Usually, since $H \ll n$, we implicitly want to learn a mapping such that \mathbf{x} is sparse with only $|x_e| \neq 0, e \in \mathcal{E}_{y_i}$. For the weight distribution of \mathbf{x} across the basis \mathcal{E}_{y_i} , we use a variant of the Tree path KL-divergence loss [27]. We first define a target distribution P over all the n nodes of \mathcal{T} by concatenating the weighted one-hot encoded vectors from all the hierarchical levels. Specifically, we define the weight distribution by the n -dimensional vector $\mathbf{w} = [w_1 \delta_1, \dots, w_h \delta_h, \dots, w_H \delta_H]^\top$, where δ_l represents a one-hot-encoded vector for the hierarchy level $l \leq h$, otherwise a zero vector. The weights are chosen to be monotonically increasing, but heavy tailed, so we use $w_l = \exp\left(\frac{1}{h+1-l}\right), l \in [h]$. The target distribution P is then obtained by normalizing the weight vector \mathbf{w} . Our first loss term is the KL divergence between the target (P) and the predicted (\hat{P}) weighted tree path distributions

$$\mathcal{L}_{kl} = \text{KL}(P \parallel \hat{P}) = \sum_{i \in [n]} P_i \log \frac{P_i}{\hat{P}_i} \quad (2)$$

where, $\hat{P}_i = \frac{e^{|\mathbf{x}_i|}}{\sum_{j=1}^n e^{|\mathbf{x}_j|}} \quad \forall i \in [n]$ is computed using the softmax function to ensure that the distance between the correct and incorrect classes is relatively high. As discussed before, the class subspaces only span at most H dimensions and therefore require \mathbf{x} to be sparse. Specifically, a leaf node at level h is only associated with h hierarchical class labels, implying that the feature vectors must span exactly one dimension for levels $l \leq h$ and zero dimensions for levels $h < l \leq H$. To achieve this, we also introduce a sparsity promoting regularization term

$$\mathcal{L}_{reg} = \sum_{l=1}^h \left\| \delta_l - \frac{\mathbb{P}_{\mathcal{E}^{(l)}} \mathbf{x}}{\|\mathbb{P}_{\mathcal{E}^{(l)}} \mathbf{x}\|} \right\|_1 + \sum_{l=h}^H \left\| \frac{\mathbb{P}_{\mathcal{E}^{(l)}} \mathbf{x}}{\|\mathbb{P}_{\mathcal{E}^{(l)}} \mathbf{x}\|} \right\|_1 \quad (3)$$

where, $\|\cdot\|_1$ represents L1-norm. The final training loss for each sample is given by $\mathcal{L}_{total} = \mathcal{L}_{kl} + \alpha \mathcal{L}_{reg}$. At the inference time, we simply pick the class using $\hat{y} = \arg \max_{y_i \in \mathcal{V}_\ell} \|\mathbb{P}_{\mathcal{E}_{y_i}} \mathbf{x}\|$.

4. Hierarchical Evaluation Metrics

Limitations of existing hierarchical metrics have been pointed out before [11]. We highlight the key gaps and propose a novel, preference-order based metric here and defer a detailed discussion to Section 9 in the supplementary.

4.1. Overview of Shortcomings

LCA distance between the true and predicted class is a key component for quantifying severity of mistakes. Most popular metrics, however, report LCA distance averaged over instances, analogous to misclassification errors in flat classification problems. Mistake Severity (MS) [5] reports average LCA of *all* misclassified instances, while [16] points out the bias in MS that leads to *better, but more* mistakes, and propose the Average Hierarchical Distance (AHD) that averages LCA distance over *all* samples – correctly and incorrectly classified – leading to a bias towards higher top-1 accuracy without adequately capturing the severity of mistakes [11]. Other metrics like hierarchical Precision (hP) and Recall (hR) have been used, but can be written as variants of a normalized version of AHD and thus suffer the same limitations. Moreover, directly using averaged LCA-based distances in the metric makes it dependent on the properties of the specific tree (e.g., height, imbalance and branching factor) and harder to interpret and compare. This difficulty is evident from the small relative differences across methods for a given dataset, and large differences across datasets while reporting MS, AHD and its @ k in experiments reported by us and others [11, 16, 20].

We consider the hierarchy tree and the specific cases presented in Fig. 2, where $D1$ is the true class and three possible prediction cases are analysed. We see that the MS and AHD@ k are unnormalized and, therefore, difficult to interpret. Moreover, AHD@ k and hP@ k deteriorate even for the best case as k increases. This also leads to a reduction of the dynamic range of the hP score, making it difficult to interpret despite being normalized. Another severe shortcoming of AHD@ k is that it computes the average LCA over the top- k predictions. Since the average is permutation invariant, the AHD@5 for the best case in Fig. 2 and a prediction instance with a much worse top-5 order as $\{C3, D4, D3, D2, D1\}$ will yield the exact same AHD@5 score. Fig. 1 also quantitatively highlights these limitations using large real-world datasets. We observe these shortcomings and note that the severity of mistakes suggests a preferred order of predicted classes. Hence, we propose a metric based on preference ordering.

4.2. Hierarchically Ordered Preference Score

Let \mathcal{U}_{d,y_c} be the set of classes at the finest level that are at LCA distance d from y_c . Note that \mathcal{U}_{0,y_c} is a singleton set with the only element being $\{y_c\}$, i.e., the correct class. We emphasize that the cost of misclassifying y_c as any of the classes in \mathcal{U}_{d,y_c} is the same, i.e., d . Therefore, an order on \mathcal{U}_{d,y_c} can be used to define the preferences of classes where any order within a set \mathcal{U}_{d,y_c} is equally preferred, i.e., the preferred ordering will be $\{\mathcal{U}_{0,y_c}, \dots, \mathcal{U}_{H,y_c}\}$. In the case when a node only has one child, for some value $d = l, \mathcal{U}_{l,y_c}$ will be empty and will be of no significance ($C2$ in Fig. 2).

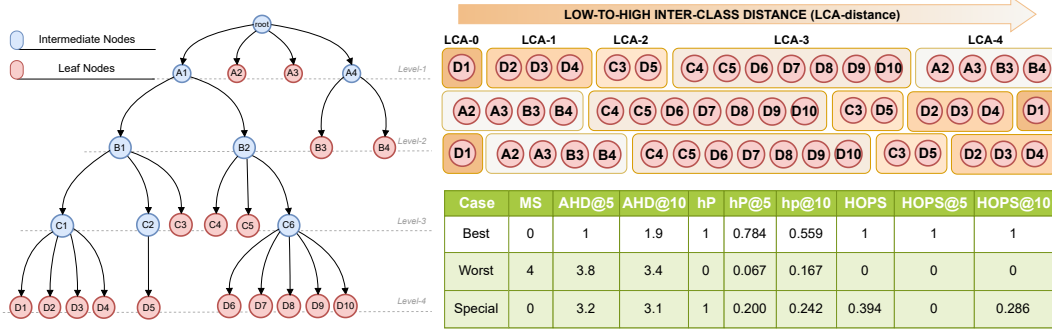


Figure 2. Best Case: The ground truth preference ordering is obtained from prediction. Worst Case: The reverse preference ordering is obtained. Special Case: The top-1 prediction is correct; however, all the other predictions are in reverse order

In order to ignore such empty sets, we use ranks instead of absolute LCA distances to represent the ordering. Specifically, we use an index set \mathbb{I} to rank all the non-empty sets in $\{\mathcal{U}_{d,y_c}\}_{d=0}^{d=H}$. We define the index set $\mathbb{I} = \{0, 1, 2, \dots, H\}$ for indexing the elements in the ordered set \mathbb{S}_{y_c} , defined as

$$\mathbb{S}_{y_c} = \{\mathbb{S}_{y_c}^i \mid i \in \mathbb{I}\} := \{\mathcal{U}_{d,y_c} \mid \mathcal{U}_{d,y_c} \neq \emptyset\}_{d=0}^{d=H}. \quad (4)$$

Now, we define the *desired order* z for a class y_c as:

$$z = [0, \underbrace{1, \dots, 1}_{|\mathbb{S}_{y_c}^1| \text{ times}}, \dots, \underbrace{k, \dots, k}_{|\mathbb{S}_{y_c}^k| \text{ times}}] \quad (5)$$

Note that this preference order is conditioned on the true class y_c . $|\mathbb{S}_{y_c}^i|$ denotes the number of classes at rank i ; therefore, z encodes the properties of the tree via ranks.

Let $\Pi = [\pi_{y_1}, \dots, \pi_{y_K}]$ be the vector of probabilities corresponding to all the leaf classes and $\hat{\Pi} = \arg \text{sort}(\Pi)$ be the vector of indices (class labels) that would sort Π in descending order. Assume $\text{rank}(y_c, y_j)$ returns the index $i \in \mathbb{I}$ of the set \mathcal{U}_{d,y_c} that contains the class y_j . Finally, we define the *obtained order* \hat{z} as follows:

$$\hat{z} = [\text{rank}(y_c, \hat{\Pi}_j)]_{j=1}^K \quad (6)$$

By defining a metric on the *desired* and *obtained* preference orders, z and \hat{z} respectively, we can derive a hierarchical metric that takes into account the branching factor and depth (or height) of the tree. Specifically, we compute the following for a single sample having the true class y_c as:

$$s = \sum_{j=1}^K \eta_j \cdot |z_j - \hat{z}_j| \quad (7)$$

where, η_j 's are defined using a multi-step exponential-linear decay function. Specifically, we use the exponential decay when the preferred rank changes, i.e., $\eta_j = 2^{-z_j}$ when j is the first occurrence of rank z_j , and for each subsequent values j for $\text{rank}=z_j$, we use a linear decay weight by linearly

interpolating between 2^{-z_j} and $2^{-(z_j+1)}$. An exponential decay ensures that the classes with higher LCA distances, when ranked closer to the predicted class, have a relatively high negative impact on the score; thereby accounting for the imbalance of the tree. Meanwhile, the linear decay accounts for the branching factor by reducing the weights for classes at the same rank as we move away from the correct class. The rationale behind the choice of this decay function is provided in Section 9 of the supplementary.

Note that we get $s_{\min} = 0$ when $z = \hat{z}$, and we use the worst possible obtained order, i.e., the reverse order of z , to get the maximum achievable score s_{\max} . The final measure of HOPS is given by:

$$\mathbf{HOPS} = 1 - \frac{s}{s_{\max}} \in [0, 1] \quad (8)$$

HOPS@ k . We are often interested in only the top- k performance of a classifier, particularly, when there are a large number of classes. We define the HOPS@ k variants, simply by modifying the notion of the worst achievable score and adapting the weights. For HOPS@ k , we define the worst ranked vector $z_r^k = [z_{k:-1:1}, z_{k+1:1:K}]$ ⁴ and the corresponding score as s_{\max}^k which is then used to compute the HOPS@K score as:

$$\mathbf{HOPS@}k = \max\left(0, 1 - \frac{s^k}{s_{\max}^k}\right) \quad (9)$$

where s^k is computed using (7), but with $\eta_{j>k} = 0$. The scores averaged over all samples are used for reporting the classifiers performance. It is worth pointing out that for $k = 1$, the HOPS@ k is different than the overall HOPS score, and that it is equal to the top-1 accuracy. This is aligned with the design of this metric, where the HOPS@ k concerns with the ranking performance of up to the k^{th} ranked prediction, while the HOPS metric concerns the complete ranking over all classes.

⁴In $z_{a:c:b}$, a is the start, b is the stop and c is the step-size

5. Results and Analysis

In this section, we summarize the results on FGVC-Aircraft [23], CIFAR-100 [17] and iNaturalist-19 [35] in Tables 1, 2 and 3, respectively. We report and analyze the results on tieredImageNet-H separately in the supplementary section. For methods denoted with an asterisk (*), we simply use the metrics reported by [11]. For each metric (column) in these tables, we highlight the cells using a color scale, where ‘white’ represents the bottom 50 percentile values and ‘green’ represents the best metric. More details on the dataset, baseline methods, backbone architectures, evaluation metrics, implementation details, training configuration and ablation are available in the supplementary.

We observe an improvement of 1.2%, 0.26% and 0.68% in the top-1 accuracy using our approach for FGVC-Aircraft, CIFAR-100 and iNaturalist-19, respectively, as compared to HAFrame [20]. The improvement in the case of ViT is 2.42%, which is a significant gain in comparison to the baseline. We also observe that, except for FGVC-Aircraft, we are competitive or better than SOTA in terms of MS across all the experiments. An interesting observation is that $K = 100$ and $n = 200$ for FGVC-Aircraft. This implies that a lot of intermediate nodes have only one child, which is also evident from the number of classes having the smallest LCA distance (1, 2, 3) are (46, 41, 13), respectively. We point out that the maximum LCA distance for FGVC-Aircraft is 3. Therefore, as also discussed in [11], this becomes a bottleneck when the existing hierarchical metrics are averaged over all the samples. Moreover, MS only considers the average cost of mistakes, and therefore, the metric is reported on different numbers of samples. Hence, it can only be compared when coupled with the top-1 accuracy. This is also evident for the ‘Soft-labels $\beta = 4$ ’ and ‘Barz & Denzler’ methods in Tables 2 and 3, respectively. To address this challenge, AHD@1 couples the top-1 performance with MS. We also observe that the reported AHD@ k metric for Hier-COS is consistently better than all the baseline methods.

We further observe that HOPS is not only consistently better across all the experimental settings for our method, but it also helps resolve the ambiguity that occurs when combining multiple metrics like top-1 accuracy, MS and AHD@ k . For instance, Flamingo-I in Table 2, as compared to HAFeat-I, has an improved top-1 accuracy and AHD@{5, 20} but a worse MS and AHD@1. Thus, it is unclear how to quantify which method is better. HOPS addresses this issue by considering not only the top-1 accuracy and severity of mistakes but also the preference order and structure of the hierarchy tree. Moreover, we observe a significant gain in the performance of Hier-COS compared to HAFrame for iNaturalist-19 because of the higher number of classes, highlighting the proficiency in learning strong hierarchical representations. While HOPS consid-

ers the preference order for all the K classes quantifying the overall hierarchical performance, it might not be useful in many real-world applications. Therefore, we also report HOPS@{5, 20} and observe that our proposed method is again consistently better than all the other methods. We further validate the richness of the hierarchy-aware feature representations by comparing the order of predictions in Fig 1. We observe that the percentage of samples with incorrect order drastically reduces for all the baselines across all the datasets. We demonstrate that our method can maintain its performance for all values of k . Additionally, we point the readers towards the evident correlation between the area under the curve (AuC) in Fig. 1 and HOPS. For instance, the MS and AHD@ k are improved for Flamingo-I and II for iNaturalist-19 compared to Cross Entropy, however, their true hierarchical performance is nearly the same in Fig. 1; therefore, they also have a similar HOPS.

Lastly, we report the FPA and HOPS on FGVC-Aircraft, CIFAR-100 and iNaturalist-19 in Table 4 along with the top-1 accuracy. We observe that the FPA is improved by 3.64% for FGVC-Aircraft, by 1.36% for CIFAR-100 and by 1.51% for iNaturalist-19, as compared to the best method, with significant gains in HOPS. We also observe that the drop in top-1 accuracy and FPA, i.e. (Accuracy - FPA), is the least in Hier-COS, thereby suggesting that our framework is hierarchically consistent. We further highlight that all the previous methods impose additional constraints in the loss function to achieve hierarchical consistency, however, our framework implicitly promotes consistency and does not require additional constraints. We also report the level-wise accuracies in Fig. 4b and 4c and observe that we perform better or competitive compared to all the baselines. Additionally, although Cross-Entropy and HAFrame do not explicitly allow classification across all the hierarchical levels, we compute the probabilities for a super-class as the sum of probabilities of all its children [11] to compare the FPA on CIFAR-100. The FPA for Cross-Entropy and HAFrame is 77.11 ± 0.002 and 77.0 ± 0.002 , respectively, which is lower than Hier-COS.

6. Discussion and Conclusion

We introduced a novel construct, the Hierarchical Composition of Orthogonal Subspaces (Hier-COS), that is inherently hierarchy-aware and naturally reduces the severity of mistakes and promotes hierarchical consistency. We propose that a rich hierarchy-aware feature representation can be learned by simply augmenting a transformation module to any deep feature extractor that can transform the learned discriminative deep embeddings into hierarchy-aware representations. To demonstrate the effectiveness of the proposed Hier-COS construction, we used a simple loss function for training and reported a comparative analysis with various baselines on challenging benchmarks with deep hi-

Method	Accuracy (\uparrow)	MS (\downarrow)	AHD@1 (\downarrow)	AHD@5 (\downarrow)	AHD@20 (\downarrow)	HOPS (\uparrow)	HOPS@5 (\uparrow)	HOPS@20 (\uparrow)
Cross Entropy	79.57 \pm 0.731	2.09 \pm 0.011	0.43 \pm 0.014	2.10 \pm 0.004	2.67 \pm 0.001	0.56 \pm 0.003	0.51 \pm 0.005	0.57 \pm 0.003
HAFrame	80.55 \pm 0.346	2.00 \pm 0.029	0.39 \pm 0.009	1.74 \pm 0.006	2.45 \pm 0.003	0.86 \pm 0.005	0.81 \pm 0.005	0.86 \pm 0.005
Hier-COS	81.75 \pm 1.006	2.09 \pm 0.029	0.38 \pm 0.020	1.73 \pm 0.009	2.44 \pm 0.003	0.89 \pm 0.007	0.84 \pm 0.010	0.88 \pm 0.007

Table 1. Results comparing the performance of hierarchical classification on the test set of FGVC-Aircraft.

Method	Accuracy (\uparrow)	MS (\downarrow)	AHD@1 (\downarrow)	AHD@5 (\downarrow)	AHD@20 (\downarrow)	HOPS (\uparrow)	HOPS@5 (\uparrow)	HOPS@20 (\uparrow)
Cross Entropy	77.77 \pm 0.248	2.33 \pm 0.014	0.52 \pm 0.007	2.25 \pm 0.007	3.19 \pm 0.004	0.54 \pm 0.001	0.05 \pm 0.001	0.17 \pm 0.001
Barz & Denzler*	68.31 \pm 0.004	2.36 \pm 0.025	0.75 \pm 0.012	1.25 \pm 0.364	2.49 \pm 0.004	-	-	-
YOLO-v2*	67.97 \pm 0.006	3.72 \pm 0.022	1.19 \pm 0.019	2.85 \pm 0.010	3.39 \pm 0.011	-	-	-
HXE+CRM*	77.63 \pm 0.280	2.30 \pm 0.026	0.51 \pm 0.009	1.11 \pm 0.008	2.18 \pm 0.003	-	-	-
Soft-labels ($\beta=30$)*	73.01 \pm 0.003	2.38 \pm 0.004	0.64 \pm 0.008	1.39 \pm 0.027	2.79 \pm 0.005	-	-	-
Soft-labels ($\beta=4$)*	67.85 \pm 0.008	2.21 \pm 0.037	0.71 \pm 0.024	1.23 \pm 0.018	2.23 \pm 0.008	-	-	-
Flamingo-I	77.87 \pm 0.137	2.31 \pm 0.026	0.51 \pm 0.007	2.06 \pm 0.016	3.08 \pm 0.006	0.57 \pm 0.002	0.09 \pm 0.004	0.21 \pm 0.004
Flamingo-II	75.26 \pm 0.508	2.32 \pm 0.029	0.57 \pm 0.017	2.41 \pm 0.007	3.29 \pm 0.017	0.51 \pm 0.003	0.03 \pm 0.001	0.14 \pm 0.004
HAFeat-I	77.51 \pm 0.224	2.24 \pm 0.025	0.50 \pm 0.006	1.43 \pm 0.009	2.64 \pm 0.003	0.69 \pm 0.001	0.41 \pm 0.007	0.47 \pm 0.004
HAFeat-II	76.47 \pm 0.219	2.27 \pm 0.019	0.54 \pm 0.008	1.70 \pm 0.012	2.84 \pm 0.007	0.63 \pm 0.001	0.22 \pm 0.005	0.32 \pm 0.001
HAFrame	77.53 \pm 0.211	2.24 \pm 0.019	0.50 \pm 0.008	1.12 \pm 0.005	2.18 \pm 0.002	0.92 \pm 0.001	0.72 \pm 0.003	0.83 \pm 0.002
Hier-CoS	77.79 \pm 0.145	2.21 \pm 0.017	0.49 \pm 0.006	1.09 \pm 0.005	2.17 \pm 0.003	0.93 \pm 0.001	0.76 \pm 0.002	0.85 \pm 0.002

Table 2. Results comparing the performance of hierarchical classification on the test set of CIFAR-100.

Method	Accuracy (\uparrow)	MS (\downarrow)	AHD@1 (\downarrow)	AHD@5 (\downarrow)	AHD@20 (\downarrow)	HOPS (\uparrow)	HOPS@5 (\uparrow)	HOPS@20 (\uparrow)
Cross Entropy	70.86 \pm 0.137	2.23 \pm 0.012	0.65 \pm 0.003	1.95 \pm 0.007	3.37 \pm 0.003	0.46 \pm 0.001	0.28 \pm 0.002	0.08 \pm 0.001
Barz & Denzler*	37.37 \pm 0.278	1.99 \pm 0.008	1.24 \pm 0.005	1.49 \pm 0.005	1.97 \pm 0.005	-	-	-
YOLO-v2*	55.83 \pm 0.046	2.43 \pm 0.001	1.10 \pm 0.001	1.50 \pm 0.001	1.99 \pm 0.002	-	-	-
HXE+CRM*	70.67 \pm 0.210	2.16 \pm 0.005	0.63 \pm 0.006	1.17 \pm 0.004	1.75 \pm 0.003	-	-	-
Soft-labels ($\beta=30$)*	58.01 \pm 0.126	2.31 \pm 0.009	0.97 \pm 0.007	1.40 \pm 0.005	1.91 \pm 0.005	-	-	-
Soft-labels ($\beta=4$)*	22.66 \pm 0.262	2.06 \pm 0.012	1.60 \pm 0.007	1.72 \pm 0.008	2.14 \pm 0.007	-	-	-
Flamingo-I	70.37 \pm 0.124	2.14 \pm 0.011	0.63 \pm 0.004	1.78 \pm 0.008	3.27 \pm 0.008	0.47 \pm 0.002	0.34 \pm 0.003	0.09 \pm 0.002
Flamingo-II	70.19 \pm 0.168	2.16 \pm 0.006	0.64 \pm 0.004	1.77 \pm 0.007	3.30 \pm 0.010	0.47 \pm 0.002	0.35 \pm 0.004	0.09 \pm 0.002
HAFeat-I	70.96 \pm 0.133	2.15 \pm 0.022	0.62 \pm 0.006	1.55 \pm 0.207	2.67 \pm 0.406	0.55 \pm 0.044	0.47 \pm 0.091	0.23 \pm 0.107
HAFeat-II	70.26 \pm 0.292	2.19 \pm 0.012	0.65 \pm 0.008	1.46 \pm 0.004	2.46 \pm 0.005	0.55 \pm 0.001	0.51 \pm 0.002	0.28 \pm 0.002
HAFrame	71.13 \pm 0.139	2.05 \pm 0.007	0.59 \pm 0.001	1.14 \pm 0.002	1.74 \pm 0.001	0.89 \pm 0.001	0.70 \pm 0.001	0.79 \pm 0.001
Hier-CoS	71.15 \pm 0.037	2.06 \pm 0.004	0.59 \pm 0.002	1.13 \pm 0.001	1.72 \pm 0.001	0.96 \pm 0.000	0.71 \pm 0.000	0.81 \pm 0.001
ViT-Cross Entropy	78.39 \pm 0.068	1.72 \pm 0.005	0.37 \pm 0.001	1.38 \pm 0.001	2.61 \pm 0.002	0.53 \pm 0.000	0.52 \pm 0.001	0.25 \pm 0.001
ViT-Hier-CoS	80.81 \pm 0.063	1.73 \pm 0.011	0.33 \pm 0.003	0.97 \pm 0.002	1.61 \pm 0.001	0.98 \pm 0.001	0.80 \pm 0.001	0.86 \pm 0.002

Table 3. Results comparing the performance of hierarchical classification on the test set of iNaturalist-19. The top partition compares the performance using ResNet-50 as the feature extractor, while the bottom partition compares the performance using a pre-trained ViT.

Method	Accuracy (\uparrow)	FPA (\uparrow)	HOPS(\uparrow)	Accuracy (\uparrow)	FPA (\uparrow)	HOPS (\uparrow)	Accuracy (\uparrow)	FPA (\uparrow)	HOPS (\uparrow)
Flamingo-I	80.71 \pm 0.408	77.92 \pm 0.579	0.58 \pm 0.004	77.87 \pm 0.137	75.19 \pm 0.333	0.57 \pm 0.002	70.37 \pm 0.124	68.63 \pm 0.139	0.47 \pm 0.002
Flamingo-II	80.07 \pm 0.364	77.70 \pm 0.641	0.57 \pm 0.005	75.26 \pm 0.508	72.43 \pm 0.336	0.51 \pm 0.003	70.19 \pm 0.168	68.75 \pm 0.163	0.47 \pm 0.002
HAFeat-I	73.30 \pm 0.361	54.38 \pm 1.718	0.53 \pm 0.002	77.51 \pm 0.224	75.52 \pm 0.223	0.69 \pm 0.001	70.96 \pm 0.133	33.36 \pm 36.553	0.55 \pm 0.044
HAFeat-II	74.53 \pm 0.592	55.73 \pm 2.676	0.53 \pm 0.009	76.47 \pm 0.219	73.24 \pm 0.208	0.63 \pm 0.001	70.26 \pm 0.292	68.01 \pm 0.256	0.55 \pm 0.001
Hier-CoS	81.74 \pm 1.000	81.56 \pm 1.020	0.89 \pm 0.007	77.79 \pm 0.145	77.37 \pm 0.118	0.93 \pm 0.001	71.15 \pm 0.037	69.93 \pm 0.028	0.96 \pm 0.000

Table 4. Hierarchical consistency on (left) FGVC-Aircraft, (center) CIFAR-100 and (right) iNat-19

erarchy trees, using CNN and ViT as backbone models. With our experiments we showed that the proposed feature space learns representations that capture the hierarchy better than the state-of-the-art. An interesting future direction of investigation would be the notion of hierarchical neural collapse [20] extended to subspaces rather than one-dimensional vectors. In Hier-COS, the relative distance between subspaces is defined based on the number of common ancestors, without assuming that the inter-class relationship is strictly a tree. We speculate that this formulation can be extended to settings where semantic relationships exist in the form of Directed Acyclic Graphs (DAGs). We provide

more insights about our framework and some of the future research directions in Section 11.

We highlighted the gaps in commonly used evaluation metrics, like MS, AHD@ k , hP and hR, and proposed a novel metric, Hierarchically Ordered Preference Score (HOPS), based on preference orderings. HOPS can also be interpreted as “a score that quantifies the weighted percentage of all the classes that are ordered according to the hierarchical preference order”. By design, HOPS@1 is equal to top-1 accuracy. We provide more insights about existing metrics in Section 9 of the supplementary. We shall publicly release our code, models and weights upon acceptance.

References

- [1] Xiang An, Xuhan Zhu, Yuan Gao, Yang Xiao, Yongle Zhao, Ziyong Feng, Lan Wu, Bin Qin, Ming Zhang, Debing Zhang, and Ying Fu. Partial fc: Training 10 million identities on a single machine. In *2021 IEEE/CVF International Conference on Computer Vision Workshops (ICCVW)*, pages 1445–1449, 2021. 1
- [2] Yalong Bai, Yuxiang Chen, Wei Yu, Linfang Wang, and Wei Zhang. Products-10k: A large-scale product recognition dataset, 2020. 1, 7
- [3] Björn Barz and Joachim Denzler. Hierarchy-based image embeddings for semantic image retrieval. In *2019 IEEE Winter Conference on Applications of Computer Vision (WACV)*, pages 638–647. IEEE, 2019. 1, 2, 3
- [4] Walter Bennette, Nathaniel Hofmann, Nathaniel Wilson, and Tyler Witter. Hierarchical open-set recognition for automatic target recognition. In *2021 IEEE Symposium Series on Computational Intelligence (SSCI)*, pages 01–08, 2021. 3
- [5] Luca Bertinetto, Romain Mueller, Konstantinos Tertikas, Sina Samangooei, and Nicholas A. Lord. Making better mistakes: Leveraging class hierarchies with deep networks. In *Proceedings of the IEEE/CVF Conference on Computer Vision and Pattern Recognition (CVPR)*, 2020. 1, 2, 3, 5, 4
- [6] Dongliang Chang, Kaiyue Pang, Yixiao Zheng, Zhanyu Ma, Yi-Zhe Song, and Jun Guo. Your “flamingo” is my “bird”: Fine-grained, or not. In *Proceedings of the IEEE/CVF Conference on Computer Vision and Pattern Recognition*, pages 11476–11485, 2021. 1, 2, 3, 7
- [7] Jia Deng, Nan Ding, Yangqing Jia, Andrea Frome, Kevin Murphy, Samy Bengio, Yuan Li, Hartmut Neven, and Hartwig Adam. Large-scale object classification using label relation graphs. In *European conference on computer vision*, pages 48–64. Springer, 2014. 2, 3
- [8] Xiwen Dengxiong and Yu Kong. Ancestor Search: Generalized Open Set Recognition via Hyperbolic Side Information Learning. In *2023 IEEE/CVF Winter Conference on Applications of Computer Vision (WACV)*, pages 3992–4001, Los Alamitos, CA, USA, 2023. IEEE Computer Society. 3
- [9] Jean Dezert, Andrii Shekhovtsov, and Wojciech Salabun. Distances between partial preference orderings, 2024. 3, 5, 6
- [10] Andrea Frome, Greg S Corrado, Jon Shlens, Samy Bengio, Jeff Dean, Marc’ Aurelio Ranzato, and Tomas Mikolov. Devise: A deep visual-semantic embedding model. In *Advances in Neural Information Processing Systems*. Curran Associates, Inc., 2013. 1, 3
- [11] Ashima Garg, Depanshu Sani, and Saket Anand. Learning hierarchy aware features for reducing mistake severity. In *Computer Vision – ECCV 2022*, pages 252–267, Cham, 2022. Springer Nature Switzerland. 1, 2, 3, 5, 7, 6
- [12] Victoria Helus, Nathan Vaska, and Natalie Abreu. Addressing mistake severity in neural networks with semantic knowledge. In *Progress and Challenges in Building Trustworthy Embodied AI*, 2022. 3
- [13] Aryan Jadon and Avinash Patil. A comprehensive survey of evaluation techniques for recommendation systems, 2024. 3
- [14] Kalervo Järvelin and Jaana Kekäläinen. Ir evaluation methods for retrieving highly relevant documents. In *Proceedings of the 23rd Annual International ACM SIGIR Conference on Research and Development in Information Retrieval*, page 41–48, New York, NY, USA, 2000. Association for Computing Machinery. 3
- [15] Carlos Nascimento Silla Jr. and Alex Alves Freitas. A survey of hierarchical classification across different application domains. *Data Min. Knowl. Discov.*, 22(1-2):31–72, 2011. 3, 4
- [16] Shyamgopal Karthik, Ameya Prabhu, Puneet K. Dokania, and Vineet Gandhi. No cost likelihood manipulation at test time for making better mistakes in deep networks. In *International Conference on Learning Representations*, 2021. 1, 3, 5, 4
- [17] Alex Krizhevsky. Learning multiple layers of features from tiny images. Technical report, 2009. 1, 3, 7
- [18] Loïc Landrieu and Vivien Sainte Fare Garnot. Leveraging class hierarchies with metric-guided prototype learning. In *British Machine Vision Conference (BMVC)*, 2021. 1
- [19] Nico Lang, Vésteinn Snæbjarnarson, Elijah Cole, Oisín Mac Aodha, Christian Igel, and Serge Belongie. From coarse to fine-grained open-set recognition. In *Proceedings of the IEEE/CVF conference on computer vision and pattern recognition*, 2024. 3
- [20] Tong Liang and Jim Davis. Inducing neural collapse to a fixed hierarchy-aware frame for reducing mistake severity. In *Proceedings of the IEEE/CVF International Conference on Computer Vision (ICCV)*, pages 1443–1452, 2023. 1, 2, 3, 4, 5, 7, 8
- [21] Shaoteng Liu, Jingjing Chen, Liangming Pan, Chong-Wah Ngo, Tat-Seng Chua, and Yu-Gang Jiang. Hyperbolic visual embedding learning for zero-shot recognition. In *Proceedings of the IEEE/CVF Conference on Computer Vision and Pattern Recognition*, pages 9273–9281, 2020. 2, 3
- [22] Qingqing Long, Yiming Wang, Lun Du, Guojie Song, Yilun Jin, and Wei Lin. Hierarchical community structure preserving network embedding: A subspace approach. In *Proceedings of the 28th ACM International Conference on Information and Knowledge Management*, page 409–418, New York, NY, USA, 2019. Association for Computing Machinery. 3
- [23] S. Maji, J. Kannala, E. Rahtu, M. Blaschko, and A. Vedaldi. Fine-grained visual classification of aircraft. Technical report, 2013. 3, 7, 1
- [24] George A Miller. *WordNet: An electronic lexical database*. MIT press, 1998. 1
- [25] Maximillian Nickel and Douwe Kiela. Poincaré embeddings for learning hierarchical representations. *Advances in neural information processing systems*, 30, 2017. 3
- [26] Vardan Papyan, XY Han, and David L Donoho. Prevalence of neural collapse during the terminal phase of deep learning training. *PNAS*, 117(40):24652–24663, 2020. 3
- [27] Seulki Park, Youren Zhang, Stella X. Yu, Sara Beery, and Jonathan Huang. Learning hierarchical semantic classification by grounding on consistent image segmentations, 2024. 1, 5

- [28] Jingtian Peng, Chang Xiao, and Yifan Li. Rp2k: A large-scale retail product dataset for fine-grained image classification, 2021. [1](#), [7](#)
- [29] Elias Ramzi, Nicolas Audebert, Nicolas Thome, Clément Rambour, and Xavier Bitot. Hierarchical average precision training for pertinent image retrieval. In *European Conference on Computer Vision*, pages 250–266. Springer, 2022. [3](#)
- [30] Joseph Redmon and Ali Farhadi. Yolo9000: better, faster, stronger. In *Proceedings of the IEEE conference on computer vision and pattern recognition*, pages 7263–7271, 2017. [1](#)
- [31] Mengye Ren, Eleni Triantafyllou, Sachin Ravi, Jake Snell, Kevin Swersky, Joshua B. Tenenbaum, Hugo Larochelle, and Richard S. Zemel. Meta-learning for semi-supervised few-shot classification. In *Proceedings of 6th International Conference on Learning Representations ICLR*, 2018. [1](#), [3](#)
- [32] Tal Ridnik, Emanuel Ben-Baruch, Asaf Noy, and Lihi Zelnik. Imagenet-21k pretraining for the masses. In *Proceedings of the Neural Information Processing Systems Track on Datasets and Benchmarks*, 2021. [1](#), [7](#)
- [33] Haokun Tian, Stefan Lattner, Brian McFee, and Charalampos Saitis. Hybrid losses for hierarchical embedding learning, 2025. [3](#), [5](#), [6](#)
- [34] Nicolas Urbani, Sylvain Rousseau, Yves Grandvalet, and Leonardo Tanzi. Harnessing superclasses for learning from hierarchical databases. In *Machine Learning and Knowledge Discovery in Databases. Research Track*, pages 247–265, Cham, 2024. Springer Nature Switzerland. [2](#), [3](#)
- [35] Grant Van Horn, Oisin Mac Aodha, Yang Song, Yin Cui, Chen Sun, Alex Shepard, Hartwig Adam, Pietro Perona, and Serge Belongie. The inaturalist species classification and detection dataset. In *Proceedings of the IEEE conference on computer vision and pattern recognition*, pages 8769–8778, 2018. [1](#), [3](#), [7](#)
- [36] Hui Wu, Michele Merler, Rosario Uceda-Sosa, and John R Smith. Learning to make better mistakes: Semantics-aware visual food recognition. In *Proceedings of the 24th ACM international conference on Multimedia*, pages 172–176, 2016. [1](#), [2](#), [3](#)
- [37] Dengyong Zhou, Lin Xiao, and Mingrui Wu. Hierarchical classification via orthogonal transfer. In *Proceedings of the 28th International Conference on International Conference on Machine Learning*, page 801–808, Madison, WI, USA, 2011. Omnipress. [3](#)

Learning and Evaluating Hierarchical Feature Representations

Supplementary Material

We provide a conceptual explanation of Hier-COS in Fig. 8 and a summary of the notations in Table 8. In Section 7, we provide details about our experimental setup and implementation details. In Section 8, we discuss the results on tieredImageNet-H. We also present the results of our ablation study and include qualitative results demonstrating the quality of feature representations learned by Hier-COS in comparison to previous methods. In Section 9, we review the existing metrics used to evaluate hierarchical classification, information retrieval and ranking systems. We formally define and discuss the limitations of each metric. In Section 11, we provide additional discussion on our framework, its complexity and some of the future research directions. We also provide additional supplementary files with our submission, which we summarize in Section 12.

7. Experimental Setup

Dataset: We evaluate our approach on the test set of four datasets: FGVC-Aircraft [23], CIFAR-100 [17], iNaturalist-19 [35] and tieredImageNet-H [31]. For FGVC-Aircraft, we adopt the original hierarchy provided by the dataset. For CIFAR-100, we use the hierarchy tree provided by [18], while for iNaturalist-19 and tieredImageNet-H, we use the hierarchies provided by [5]. The statistics of these datasets are summarized in Table 5.

Dataset	H	K	n	Train	Val	Test
FGVC-Aircraft	3	100	200	3.3K	3.3K	3.3K
CIFAR-100	5	100	134	45K	5K	10K
iNaturalist-19	7	1010	1189	187K	40K	40K
tieredImageNet-H	12	608	842	425K	15K	15K

Table 5. Statistics of the datasets while excluding the root node. H is the height of the hierarchy tree, K is the number of fine-grained classes and n is the total number of nodes in the tree. The right-most three columns represent the approximate number of samples in train, val and test sets, respectively.

Baseline Methods: We compare our method with [3, 5, 6, 11, 20, 30] and a *flat* cross-entropy-based classification approach. Following [20], we also include baselines without the transformation layer (I) and with the transformation layer (II). For a fair comparison with the best competing methods, we re-did the experiments using the official code-base provided by the authors. For methods denoted with an asterisk (*), we simply use the metrics reported by [11]. Among all the baseline methods, [6, 11] train an additional classifier for each level of granularity. We compare our results with them to evaluate hierarchical consistency. Al-

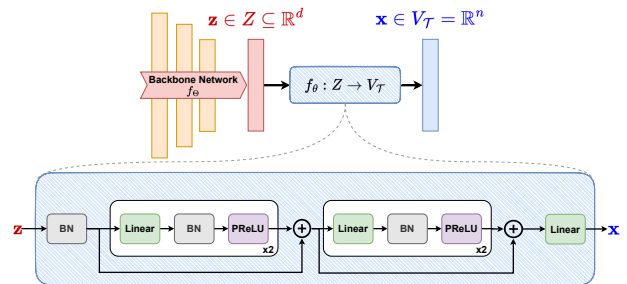


Figure 3. Illustration of the transformation module $f_\theta : Z \rightarrow V_T$. The components of f_θ are inspired from HAFrame [20]

though cross entropy and [20] do not explicitly allow classification across all the hierarchical levels, we compute the probabilities for a super-class as the sum of probabilities of all its children to compare the FPA on CIFAR-100 [11]. None of the previous methods evaluate the hierarchical performance of a transformer-based method. We create a simple baseline where we only fine-tune the output layer of a pre-trained ViT using the cross-entropy loss.

Backbone Architectures: Following the same strategy as [11, 20], we use WideResNet architecture for CIFAR-100 and ResNet-50 for FGVC-Aircraft, iNaturalist-19 and tieredImageNet-H. In addition to the CNN-based feature extractors, we compare our method using a transformer-based backbone. We use pre-trained a ViT-MAE for iNaturalist-19 as the feature extractor and freeze the weights, i.e., we only learn a transformation map from the learned embedding space to Hier-COS.

Evaluation Metrics: We follow the same evaluation strategy as [5, 11, 16, 20] and report the top-1 accuracy, MS and AHD@{1, 5, 20} for all the baseline methods. Similar to [20], we report the mean and 95% confidence interval derived from the t-distribution with four degrees of freedom for five different seeds. Additionally, we report the proposed HOPS, HOPS@{5, 20} for the competing methods. To quantify hierarchical consistency, we also report the full-path accuracy (FPA) [27] for FGVC-Aircraft, CIFAR-100 and iNaturalist-19. We do not report FPA for tieredImageNet-H because the leaf classes in the corresponding hierarchy tree are not at the same level. Unlike previous methods, we do not artificially extend the leaf nodes to be at the same level, therefore, classes at levels $l \in [H]$ are not well defined.

Method	Accuracy (\uparrow)	MS (\downarrow)	AHD@1 (\downarrow)	AHD@5 (\downarrow)	AHD@20 (\downarrow)	HOPS (\uparrow)	HOPS@5 (\uparrow)	HOPS@20 (\uparrow)
Cross Entropy	73.63 \pm 0.312	6.95 \pm 0.021	1.83 \pm 0.023	5.66 \pm 0.008	7.29 \pm 0.010	0.58 \pm 0.001	0.23 \pm 0.003	0.14 \pm 0.002
Barz & Denzler*	60.27 \pm 0.240	6.80 \pm 0.019	2.70 \pm 0.022	5.48 \pm 0.271	6.21 \pm 0.005	-	-	-
YOLO-v2*	66.02 \pm 0.099	6.99 \pm 0.011	2.38 \pm 0.012	5.05 \pm 0.001	6.17 \pm 0.001	-	-	-
HXE+CRM*	73.54 \pm 0.150	6.89 \pm 0.027	1.82 \pm 0.016	4.82 \pm 0.006	6.03 \pm 0.004	-	-	-
Soft-labels ($\beta=30$)*	69.31 \pm 0.125	6.99 \pm 0.007	2.15 \pm 0.008	4.95 \pm 0.001	6.11 \pm 0.001	-	-	-
Soft-labels ($\beta=4$)*	17.28 \pm 0.079	7.54 \pm 0.001	6.24 \pm 0.005	6.94 \pm 0.005	7.25 \pm 0.002	-	-	-
Flamingo-I	72.27 \pm 0.209	6.96 \pm 0.016	1.93 \pm 0.017	5.77 \pm 0.010	7.42 \pm 0.012	0.58 \pm 0.001	0.22 \pm 0.001	0.13 \pm 0.002
Flamingo-II	65.72 \pm 1.551	7.07 \pm 0.036	2.42 \pm 0.122	5.79 \pm 0.023	7.33 \pm 0.018	0.58 \pm 0.001	0.22 \pm 0.004	0.14 \pm 0.002
HAFeat-I	73.49 \pm 0.218	6.92 \pm 0.027	1.83 \pm 0.016	5.55 \pm 0.020	6.98 \pm 0.017	0.65 \pm 0.003	0.28 \pm 0.002	0.21 \pm 0.003
HAFeat-II	67.89 \pm 1.772	7.05 \pm 0.016	2.26 \pm 0.128	5.62 \pm 0.036	6.97 \pm 0.015	0.65 \pm 0.004	0.26 \pm 0.011	0.20 \pm 0.007
HAFrame	73.70 \pm 0.284	6.90 \pm 0.007	1.82 \pm 0.019	4.96 \pm 0.013	6.16 \pm 0.009	0.87 \pm 0.003	0.56 \pm 0.008	0.60 \pm 0.009
Hier-CoS	72.22 \pm 0.211	6.70 \pm 0.009	1.86 \pm 0.012	4.81 \pm 0.006	6.02 \pm 0.002	0.94 \pm 0.001	0.71 \pm 0.003	0.76 \pm 0.002

Table 6. Results comparing the performance of hierarchical classification on the test set of tieredImageNet-H.

7.1. Implementation Details

Inspired by HAFrame [20], the transformation module comprises of 5 linear layers, each with hidden units same as the number of nodes n , along with batch-norm layer and PReLU activation feeding to a fully connected layer with fixed weights $\{e_1 \dots, e_n\}$ (Fig. 3). A small distinction from [20] is that we define the transformation module f_θ as the Transformation + Linear module of HAFrame. We re-emphasize that the weight vectors (equivalently, the basis set \mathcal{E}) can be arbitrary but are always orthonormal and fixed for the fifth linear layer.

7.2. Training Configuration

We use the same training configurations as [20]. We obtained the best results on FGVC-Aircraft, CIFAR-100, iNaturalist-19 and tieredImageNet-H using α as (0.1, 0.05, 0.001, 0.0001), respectively. To compare our method using a transformer-based backbone, we freeze the weights of the backbone and only fine-tune f_θ for 10 epochs with $\alpha = 1e - 4$.

8. Additional Experiments and Results

We summarize the results on tieredImageNet-H in Table 6. We observe a reduction of 1.48% in the top-1 accuracy as compared to SOTA, while we observe significant improvements in MS, AHD@{5, 20}, HOPS and HOPS@{5, 20}. AHD@1 is slightly reduced because of the degraded top-1 performance. We emphasize that tieredImageNet has a complex hierarchical structure (visualized in *Results and Analysis.pdf*) with leaf nodes at different levels of the hierarchy. This makes learning algorithms difficult to optimize. This is also evident in SOTA. We observe that while HAFrame improves the top-1 performance, its overall performance is not better than the baseline HXE+CRM. The AHD@ k metrics for HXE+CRM are significantly better than HAFrame, while we show that with a slight reduction in top-1 performance, Hier-COS is able to achieve better performance across all the hierarchical metrics.

Fig. 1 also depicts the improvement in hierarchical per-

formance. We observe a huge drop in the percentage of samples with correct prediction orders using all the previous methods for all $k > 1$ in Fig. 1. Although the drop in accuracy is not justified because, unlike [5], we demonstrated via other experiments that there is no trade-off between top-1 and hierarchical performance, we speculate that this occurs due to the design of a simple loss function that does not account for the imbalance in the height of subtrees. Specifically, each class in tieredImageNet-H spans a different number of dimensions, while all the classes in other datasets span exactly H dimensions. We hypothesize that accounting for the dimensionality of subspaces should also improve the top-1 accuracy.

8.1. Ablative Study

In this section, we examine the (i) impact of the regularization term (Fig. 4a), (ii) the effect of adding extra dimensions to the vector space (Fig. 4b and 4c) and (iii) the influence of α on the hierarchical performance (Table 7). In Fig. 4a, we plot the percentage of samples with correct order for the top- k predictions against k . We observe that when \mathcal{L}_{reg} is not used (dotted line), the hierarchical performance reduces with k , however, it is still better than the previous methods shown in Fig. 1. Including \mathcal{L}_{reg} minimizes the norm of the projection of a feature vector corresponding to a class y_i onto its complementary subspace $V_i^\perp = \text{span}(\mathcal{E} \setminus \mathcal{E}_{y_i})$. Therefore, we would expect the feature vector to be closer to the subspace corresponding to the correct class y_i . We validate this on CIFAR-100 by calculating the cosine similarity between \mathbf{x} and $\mathbb{P}_{\mathcal{E}_{y_i}} \mathbf{x}$. The cosine similarity obtained with and without \mathcal{L}_{reg} is 0.97 and 0.87, respectively.

In Fig. 4b and 4c, we observe that when no additional dimensions are added to the vector space, i.e., $V_i = \text{span}(\{e_i\})$, the level-wise accuracy is competitive with the proposed Hier-COS framework (i.e., $V_i = \text{span}(\mathcal{E}_i)$); however, the HOPS metric is deteriorated significantly. This suggests that extra dimensions help in learning diverse and discriminative features across all the hierarchical levels. Further, we emphasize that, unlike [6, 11], a single classifier is used to predict classes across all the levels. This demon-

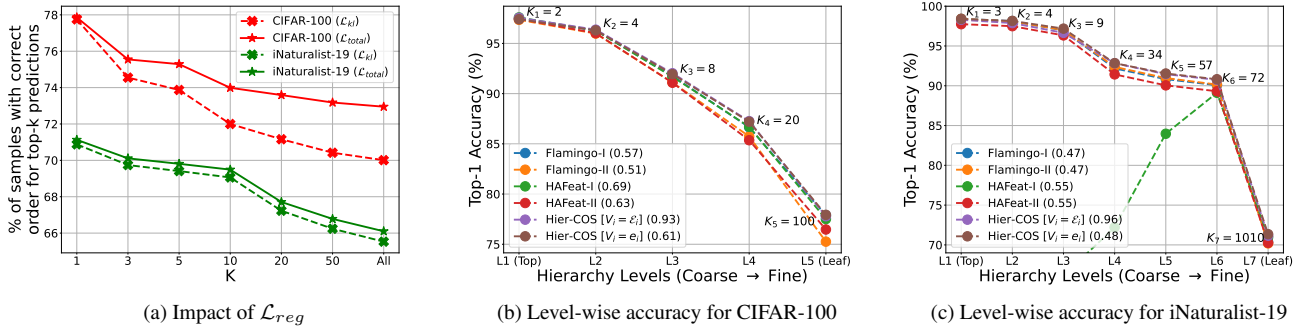


Figure 4. Ablative analysis examining (a) the impact of the regularization term and (b, c) the effect of adding extra dimensions to V_i . HOPS metric is mentioned in parenthesis in (b, c).

strates that learned feature representations are generalized across all the hierarchical levels. We discuss this property further in Section 11.

Finally, we evaluate the performance of Hier-COS in Table 7 with different values of α on CIFAR-100. We observe that the performance is not too sensitive to α and maintains the same hierarchical performance across all the values with slight variations in top-1 accuracy.

α	Accuracy	MS	AHD@5	AHD@20	HOPS
0	77.51 \pm 0.288	2.21 \pm 0.026	1.10 \pm 0.005	2.17 \pm 0.002	0.93 \pm 0.001
5e-2	77.79 \pm 0.145	2.21 \pm 0.017	1.09 \pm 0.005	2.17 \pm 0.003	0.93 \pm 0.001
1e-2	77.39 \pm 0.231	2.21 \pm 0.049	1.10 \pm 0.010	2.18 \pm 0.004	0.93 \pm 0.002
5e-3	77.43 \pm 0.072	2.21 \pm 0.008	1.10 \pm 0.002	2.18 \pm 0.002	0.93 \pm 0.001
1e-3	77.48 \pm 0.371	2.22 \pm 0.020	1.10 \pm 0.006	2.18 \pm 0.004	0.93 \pm 0.002
1e-4	77.41 \pm 0.217	2.23 \pm 0.019	1.11 \pm 0.005	2.18 \pm 0.004	0.93 \pm 0.001

Table 7. Sensitivity Analysis of α on CIFAR-100

8.2. Qualitative Analysis

In this section, we demonstrate that our method learns stronger hierarchical feature representations as compared to the previous methods. Fig. 1 only highlights the overall hierarchical performance of the methods, where even a small mistake would result in an error. For a deeper analysis of the learned representations, for all the samples belonging to a class y_i , we visualize the average of the log probabilities for the complete prediction vector comprising of K classes. A higher log probability denotes a higher preference (or a low inter-class distance). We explain these plots using the ground truth LCA-based log probabilities on the test set of CIFAR-100 in Fig. 5, representing the best hierarchical performance, and demonstrate the hierarchical performance across all the datasets in Fig. 6. We observe that Hier-COS is able to learn better hierarchical representations than any of the other baseline methods.

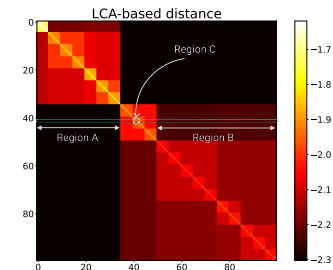


Figure 5. Ground truth LCA-based log probabilities on the test set of CIFAR-100 representing the best hierarchical performance. Consider the row highlighted by the rectangular box, say class y_c . ‘Region A’ contains the classes farthest from the class y_c because they have the least log probability in that row. Similarly, ‘Region B’ contains all the classes closer to y_c than the classes in ‘Region A’ but are farther than all the other classes that are not in ‘Region A’ and ‘Region B’. ‘Region C’ contains only one class, i.e., y_c , and represents the average log probability of being correct. The color scale of log probabilities helps in understanding the hierarchical preference order. Therefore, for learned hierarchy-aware feature representation, we would expect the log probabilities to follow a similar preference order.

9. A Review of Evaluation Metrics

This section discusses some of the widely used and related evaluation metrics for hierarchical classification methods. This also includes metrics used for evaluating information retrieval and recommendation systems.

9.1. Definitions

Mistake Severity: The severity of a mistake is often quantified using the hierarchical distance of a mistake, i.e., the LCA distance between the ground truth and the predicted class when the input is misclassified [5].

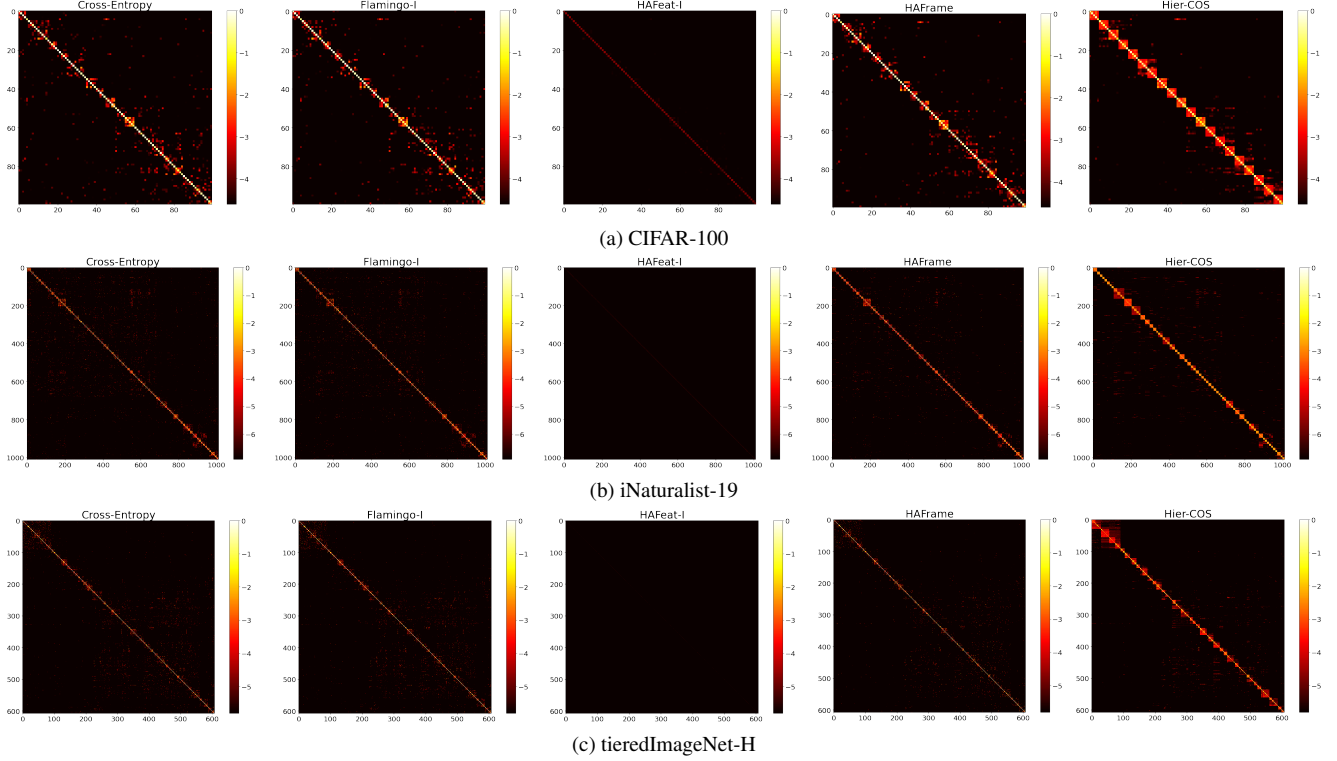


Figure 6. Plots showing the obtained order from different classification methods on the test set of (a) CIFAR-100, (b) iNaturalist-19 and (c) tieredImageNet-H. The rows and columns represent the K classes. Each row contains the softmax-based log probabilities for all the K classes averaged over all the samples belonging to that class. All the classes are grouped according to the LCA distance.

$$MS = \frac{1}{FP + FN} \sum_{i=1}^{|\mathcal{X}|} height(LCA(y_i, \hat{y}_i))$$

where y_i and \hat{y}_i are the ground truth and the predicted class label at the finest level of granularity for a sample i in the dataset and $|\mathcal{X}|$ is the total number of samples in the dataset \mathcal{X} . The MS is averaged over all misclassifications, i.e., the total number of false positives (FP) and false negatives (FN). It is important to note that the hierarchical distance for correct predictions is zero, and hence, averaging it over only FP and FN makes it equivalent to saying that MS is computed for misclassified samples only.

Average Hierarchical Distance @ k : A major drawback of the MS metric was pointed out by [16] that it only considers the misclassified samples and hence needs to be paired with top-1 accuracy for comparing different methods. A simple extension of MS is to average over all the samples $|\mathcal{X}|$ instead of only the misclassified ones (FP + FN) [5].

$$AHD = \frac{1}{|\mathcal{X}|} \sum_{i=1}^{|\mathcal{X}|} height(LCA(y_i, \hat{y}_i))$$

In the case of hierarchy-aware feature representations, we would expect not only lower MS and AHD values but also smaller LCA distances between the top predictions – an aspect that neither MS nor AHD adequately captures. Therefore, [5] also proposes to compute the average AHD for all the top- k predictions, defined as:

$$AHD@k = \frac{1}{|\mathcal{X}|} \sum_{i=1}^{|\mathcal{X}|} \frac{1}{k} \sum_{j=1}^k height(LCA(y_i, \hat{y}_{ij}))$$

where \hat{y}_{ij} is the top- j^{th} ranked prediction for sample i .

Hierarchical Precision and Recall: For evaluating hierarchical classification methods, hierarchical precision (hP) is used, which is the proportion of correctly predicted classes among all the predicted classes at all the hierarchical levels,

$$hP = \frac{1}{|\mathcal{X}|} \sum_{i=1}^{|\mathcal{X}|} \frac{|\tilde{f}_a(v_{\hat{y}_i}) \cap \tilde{f}_a(v_{y_i})|}{|\tilde{f}_a(v_{\hat{y}_i})|}$$

where y_i and \hat{y}_i are the ground truth and predicted class labels, respectively, v_{y_i} and $v_{\hat{y}_i}$ are the corresponding nodes in the tree and $\tilde{f}_a(v_i)$ is the set containing all the ancestors of v_i and itself, i.e., $\{f_a(v_i) \cup v_i\}$ [15].

Similarly, for any sample i , hierarchical recall (hR) is the proportion of correctly predicted classes among all the ground truth classes at all the hierarchical levels.

$$hR = \frac{1}{|\mathcal{X}|} \sum_{i=1}^{|\mathcal{X}|} \frac{|\tilde{f}_a(v_{\hat{y}_i}) \cap \tilde{f}_a(v_{y_i})|}{|\tilde{f}_a(v_{y_i})|}$$

In simpler words, we can say that hR is analogous to hP but focuses on how well the true hierarchical structure is retrieved rather than the correctness of the predicted structure.

Total Preference Ordering: We often deal with information expressed as partial orderings (PO). For PO based on a hierarchy tree, the highest preference is given to the ground truth class, the second highest to all its siblings, the third highest to all its first cousins, and so on, resulting in a total preference ordering (TPO) [9]. There could also be other TPOs, such as TPO based on the prediction probabilities. [9] presents a metric to compare TPOs using a pair-wise Preference-Score Matrix (PSM), M , for each TPO, defined as:

$$M(i, j) = \begin{cases} 1, & \text{if } x_i \succ x_j, \\ -1, & \text{if } x_i \prec x_j, \\ 0, & \text{if } x_i = x_j. \end{cases}$$

where x_i and x_j denote the preference scores of a classes i and j , respectively, and $M(i, j)$ is the component of PSM representing whether the classes i and j are in the correct preference order. Finally, [9] defines the distance between the two TPOs using the Frobenius distance as follows:

$$d_F(M_1, M_2) = \|M_1 - M_2\|_F \\ = \sqrt{\text{Tr} \left((M_1 - M_2)^T (M_1 - M_2) \right)}$$

Mean Reciprocal Ratio and Normalized Rank: A popular evaluation metric used in information retrieval and ranking systems is Mean Reciprocal Rank (MRR). We present its definition with respect to our problem setup. As the name suggests, it measures the mean of the reciprocal of the ranks for the correct class. Specifically, rank can be considered as the position or index at which the correct class appears in an ordered list of predictions. The lowest rank, zero, signifies the prediction with the highest confidence.

$$MRR = \frac{1}{|\mathcal{X}|} \sum_{i=1}^{|\mathcal{X}|} \frac{1}{rank_i}$$

Recently, Tian et al. [33] proposed an alternative to MRR for hierarchical classification called Mean Normalized Rank (MNR). We present its definition with respect to multi-class classification below:

$$MNR = \frac{1}{|\mathcal{X}|} \sum_{i=1}^{|\mathcal{X}|} \left(\frac{1}{H} \sum_{l=1}^H \left(\frac{rank_i^l}{K_l} \right) \right)$$

In simpler words, MNR is the average rank over all the hierarchical levels normalized by the number of classes at each level.

Normalised Discounted Cumulative Gain: Normalized Discounted Cumulative Gain (NDCG) is a standard metric that evaluates the quality of recommendation and information retrieval systems. NDCG measures the ability of a method to sort items based on relevance. The relevance score is inversely proportional to ranks, i.e., the higher relevance score is better. The $NDCG@k$ computes the NDCG for top- k predictions, given for each sample i by:

$$NDCG_i@k = \frac{DCG_i@k}{IDCG_i@k} \\ DCG_i@k = \sum_{j=1}^k \frac{rel_{i,j}}{\log_2(j+1)}$$

where, $IDCG@k$ is the $DCG@k$ for the ideal ranking. Recently, Tian et al. [33] presented an approach to extend this metric to hierarchical classification, where relevance between classes i and j is defined based on the structure of the hierarchy tree as:

$$rel_{i,j} = 1 - \frac{d(i, lca(i, j)) + d(j, lca(i, j))}{D_{\mathcal{T}}}$$

where, i is the ground truth class, j is the predicted class, $lca(i, j)$ is the lowest common ancestor between i and j , $d(i, j)$ is the number of edges between the nodes i and j , and $D_{\mathcal{T}}$ is the length of the longest path between any two leaf nodes.

9.2. Limitations

Mistake Severity: We emphasize that MS only considers the average cost of mistakes and is biased towards methods that make *more* mistakes in numbers but less in severity [16]. Therefore, it can only be compared when coupled with the top-1 accuracy. This is also evident for the ‘Soft-labels $\beta = 4$ ’ and ‘Barz & Denzler*’ methods in Tables 2 and 3, respectively. Moreover, the metric is dependent on the properties of the tree and is not normalized. Because the MS is unnormalized, this is often interpreted as the average LCA distance for a mistake. However, for a given class, the lowest MS for misclassification is dependent on the LCA

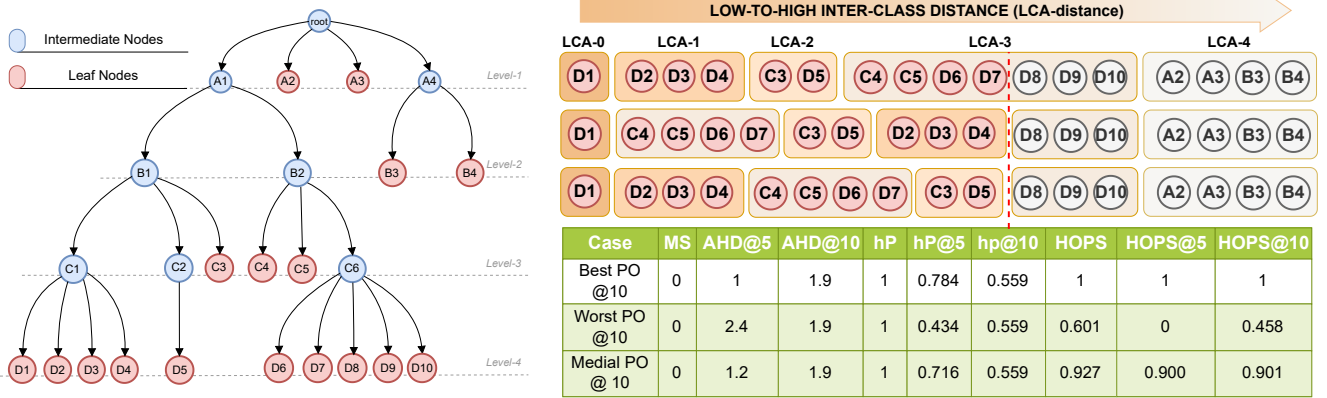


Figure 7. (Left) The same taxonomy \mathcal{T} shown in Fig 8. (Right) Three examples with correct prediction but varying top-10 predictions.

distance of the nearest sibling, which results in a higher MS for imbalanced trees, even for less severe mistakes. For instance, whenever classes $A2$ and $A3$ of the taxonomy \mathcal{T} in Fig 7 are misclassified, the MS is expected to be high because most incorrect classes are at a higher LCA distance. Therefore, we discover that MS depends on the leaf node’s depth, tree’s branching factor and imbalance, and it is challenging to interpret the MS score without due consideration to the tree structure.

AHD@ k : AHD@1 can be viewed as a straightforward extension of MS that does not require pairing with top-1 accuracy. However, as highlighted by [11], this metric tends to be biased towards higher top-1 accuracy and fails to effectively measure the severity of mistakes. Moreover, similar to MS, AHD@ k is also unnormalized and suffers from the limitations discussed above. For instance, although the predictions are correct, AHD@{5, 10} is non-zero for all the cases in the Fig. 7, which depends on the structure of the tree. Moreover, the average operation is permutation invariant; therefore, any random permutation of the same top- k prediction results in the same AHD@ k . For instance, AHD@10 for any random permutation of the top-10 predictions is always 1.9, as shown in Fig. 7. Therefore, we discover that AHD@ k also depends on the properties of the tree and is invariant to the order of predictions.

hP and hR: Similar to AHD@ k , we can also use the average hP and hR of the top- k predictions to get hP@ k and hR@ k , respectively. Both hP@ k and hR@ k can be viewed as alternatives to AHD@ k that are normalized. Observe that $|\tilde{f}_a(v_{\hat{y}_i}) \cap \tilde{f}_a(v_{y_i})|$ measures the LCA similarity between the ground truth and the predicted classes, i.e., as the number of common nodes increases the similarity increases; therefore, a higher value represents better performance. However, because of their resemblance to AHD@ k , both possess similar limitations, i.e., both depend on the tree’s properties and are permutation invariant. Moreover, for a balanced tree having the leaf nodes at the same level,

we know that $|\tilde{f}_a(v_{\hat{y}_i})| = |\tilde{f}_a(v_{y_i})|$, therefore, $hP = hR$. In Fig 7, it is evident that hP@ k is a normalized version of AHD@ k . **TPO:** This metric fundamentally depends on the definition of TPOs and their corresponding PSMs. We can use the hierarchy tree to define a ground truth PSM, say M_1 . However, determining an order of preferences from the prediction is not well-defined when we have multiple classes at the same preference value, which is almost always the case with hierarchies. Therefore, although [9] presents a promising direction to compare the TPOs, it is not yet feasible for hierarchical evaluations. Even if we assume a method exists to determine the order of preferences from the prediction, using this method for hierarchical evaluation is still challenging. The construction of PSM considers all misclassifications equally severe. Moreover, deciding which classes (based on ground truth TPO) are more important when considering a hierarchy with a huge number of leaf nodes is often important.

MRR and MNR: MRR only considers the rank of the correct prediction, while ignoring all the negative classes. Therefore, it is analogous to AHD@1 and, hence, suffers from the same problems. Similarly, MNR is also computed over the correct prediction at all levels and has the same limitations. Further, MNR requires a ranking over all the hierarchical levels. Hence, it can not be used for methods that predict for a single level, like Cross-Entropy and HAFrame. **NDCG@ k :** The definition of the relevance given by [33] does not hold for trees that do not have leaf nodes at the same level. According to them, $d(D1, A2) < d(D1, D6)$ in Fig 2, however, we can see that $D1$ is closer to $D6$ than $A2$. Moreover, the discounting factor, $\frac{1}{\log_2(j+1)}$ for each class with rank j , is independent of the hierarchical structure. Therefore, NDCG@ k does not capture the properties of the hierarchy tree. Specifically, for a class that has all the nearest- k neighbors at the same LCA distance, if the predicted class at $(k-1)^{\text{th}}$ rank has a higher LCA distance, the penalty is decayed significantly ($\frac{1}{\log_2(k)}$) without consider-

ing that all the top- k predictions are equally relevant.

10. HOPS: An example

As discussed in the previous section, for a given ground-truth class y_c , we get a *preference order* based on the hierarchy tree by constructing z as:

$$z = [0, \underbrace{1, \dots, 1}_{\times n_1}, \dots, \underbrace{k, \dots, k}_{\times n_k}] \quad , \quad k \leq H \quad (10)$$

where, n_k denotes the number of $(k-1)^{th}$ -nearest higher order cousins of class y_c and $n_0 = 1$ (self). This implies that z is the *desired* preference ordering where all the classes are arranged according to the hierarchy-based preferences such that a lower value of z_j denotes a higher preference (similar to ranks). We then propose to construct \hat{z} using the predictions such that it contains the preference values of the predicted classes based on \mathbf{z} . For instance, z and \hat{z} corresponding to the second row in Fig 7 will be:

$$\begin{aligned} z &= [0, 1, 1, 1, 2, 2, 3, 3, 3, 3, 3, 3, 4, 4, 4, 4] \\ \hat{z} &= [0, 3, 3, 3, 3, 2, 2, 1, 1, 1, 3, 3, 4, 4, 4, 4] \end{aligned}$$

11. Additional Discussions

Why Span of Subspaces instead of Union of Subspaces?

Consider two leaf classes A and B , and the vectors belonging to their corresponding subspaces, i.e. $\mathbf{x}_A \in V_A$ and $\mathbf{x}_B \in V_B$. Note that a union of these subspaces $U = V_A \cup V_B$ is not a vector space, but defines that a feature vector can either be contained completely in V_A or completely in V_B , i.e., $\mathbf{x}_A + \mathbf{x}_B \notin U$. This formulation is indeed theoretically relevant for the Hier-COS framework as we do not want the feature vectors to span the dimensions that do not belong to $f_a(\cdot)$ and $f_b(\cdot)$. However, in a learning framework, we often leverage softmax based probabilities that map logits $|x_i| \forall i \in [n]$ to probability scores \hat{p}_i and are always positive. Therefore, the condition for a union of subspaces will be violated and the feature vectors will span the corresponding subspaces, i.e., $\mathbf{x} \in \text{span}(V_A \cup V_B)$. In the case of learning frameworks that do not involve softmax, additional constraints will be required to introduce, however, we speculate that the assumptions for a union of subspaces will be easily violated. Further, we emphasize that a union of subspaces is the ideal solution that we target to achieve, however is not necessarily required to learn a hierarchy-aware feature representation. Therefore, we chose to define the framework using the span of subspaces. **Learning From Leaves, Using for All:** Hier-COS is a framework that allows learning of strong hierarchical feature representations using a transformation module f_θ . This transformation module maps feature vectors from deep network embedding space Z to a fixed orthonormal frame. The

transformation module is learned using the leaf classes and, therefore, effectively training a single classifier. We emphasize that although we learn the transformation module (classifier) for the finest classes only, we can use the same transformation module to predict classes at any of the H hierarchical levels.

Automatic Adjustment of Dimensionality based on Hierarchical Structure: Consider a binary tree consisting of one leaf node as the left subtree and a dense tree with $K-1$ leaf nodes as the right subtree. This implies that the intra-class variance of the left subtree is very low as compared to the right subtree. Therefore, to accommodate for the complex intra-class variation of the right subtree, the design of Hier-COS automatically adjusts the dimensionality of the subspace. The dimensionality of a subspace corresponding to any node in the Hier-COS framework is directly proportional to the total number of ancestors and descendants in the tree.

Computational Overhead: In the worst case, the complexity for a complete b -ary tree is $\mathcal{O}(\frac{bK-1}{b-1}) \approx \mathcal{O}(K)$. However, in the real world, the complexity is much lower because the hierarchy trees are rarely complete. The values of (K, n) for all the datasets is given in table Table 5. Moreover, unlike Flamingo and HAFeat, we do not append dummy nodes to have all the leaf nodes at the same level. Additionally, we do not train separate classifiers for each hierarchical level. Hence, we are resource-efficient when compared to these methods.

Reducing Complexity when Severity of Mistakes is not important: The ablation experiments suggested that the level-wise accuracy for all the datasets is maintained even when the subspaces are defined using $V_i = \text{span}(\{e_i\})$, while the severity of mistakes is compromised. This is because all the leaf classes are orthogonal and have no hierarchical awareness. As mentioned earlier, the Hier-COS framework learns a single classifier that is capable of classifying at all levels, we can reduce the complexity of the network if the severity of mistakes is not concerned. Specifically, for predicting classes at level l , we can prune the network by removing all the weights corresponding to $\{\mathcal{E} \setminus \mathcal{E}^{(l)}\}$.

Extending to DAGs and Arbitrary Groups: Previous methods [6, 11] learn the semantic relationship between the leaf classes by learning a separate classifier for every level in the hierarchy tree using a multi-class classification loss with additional constraints. However, in case the relationship is not represented as a tree [2, 28, 32], these methods can not be used and are non-trivial to extend. HAFrame [20] fixes the frames based on the LCA distance between leaf nodes. However, in the case of a Directed Acyclic Graph (DAG), there can be multiple lowest common ancestors that makes this formulation ambiguous and non-trivial to apply in such a setting. In contrast, we formulate Hier-

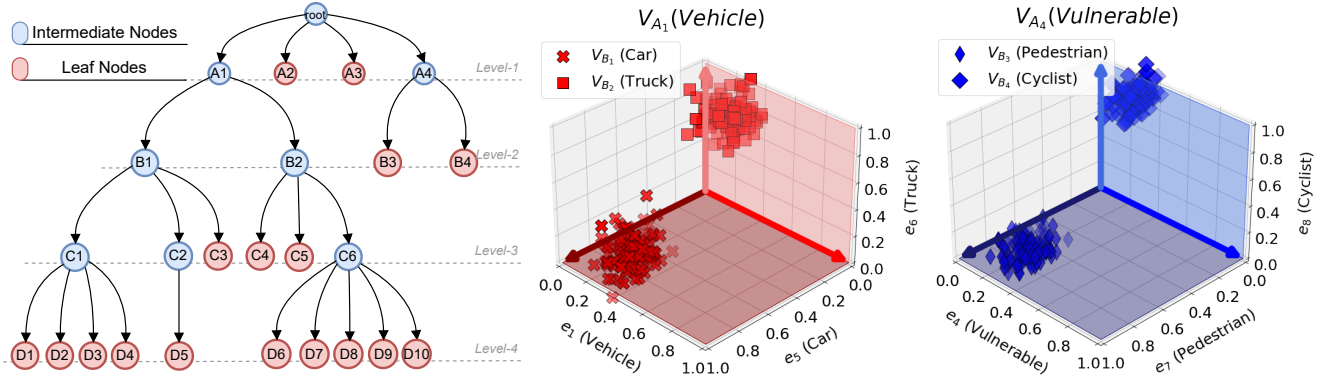


Figure 8. Consider the taxonomy \mathcal{T} (left) and its disjoint subtrees rooted at $\{A_1, A_2, A_3, A_4\}$ at level-1. We propose that these disjoint subtrees should be mapped to complementary subspaces. For instance, since A_1 and A_4 are unrelated, they should be mapped to complementary subspaces, as shown in figures (center) and (right) depicting the complementary 3D subspaces. This approach extends to deeper levels, so that disjoint subtrees at level-2 (rooted at nodes $\{B_1, B_2, B_3, B_4\}$) are also mapped to complementary subspaces, and so forth. However, applying this rule strictly at all levels would lead each fine-grained class to be orthogonal to every other class, which is not our goal. Therefore, to respect the hierarchical relationships, we propose the Hierarchical Composition of Orthogonal Subspaces (Hier-COS) framework, which learns to map deep network embeddings into a vector space that aligns with the structure of the label hierarchy tree. Specifically, we assign a unique orthonormal basis vector to each node in \mathcal{T} and define the subspace for each node as the span of the basis vectors associated with itself, its ancestors (excluding the root), and all its descendants. For example, feature vectors belonging to class B_3 are contained not just within the span of e_7 but within the plane spanned by e_4, e_7 , as shown in fig (right). This construction ensures that semantically related classes are closer in the feature space by sharing common ancestor nodes, which translates into a higher overlap of subspaces for more closely related classes.

COS based on the number of common ancestors between any two leaf nodes, which is unambiguous for DAGs or any arbitrary grouping that defines the hierarchical structure.

Designing Kernel Tricks: Kernel methods have been widely used in various domains as they allow embeddings to be learned in a very high dimensional space while actually operating in a lower dimensional feature space. At the core, kernel methods use kernel functions that compute the inner product in a lower-dimensional feature space while implicitly transforming the feature embeddings into a higher-dimensional vector space where patterns become easier to recognize. We re-iterate that Hier-COS is a framework that defines a vector space $V_{\mathcal{T}}$ which implicitly captures the properties of the hierarchical structure. Therefore, we hypothesize that kernel tricks can be designed for implicitly transforming the feature vectors from Z into $V_{\mathcal{T}}$ without operating in the n -dimensional vector space. This will especially be beneficial when the number of leaf nodes is very high and the given semantic relationship is complex.

12. Additional Supplementary

This section summarizes all the supplementary files shared with the main paper. In *Results and Analysis.pdf*, we share pre-computed results of our analysis on CIFAR-100. It includes visualization of hierarchy trees for all the datasets (demonstrating the complexity, imbalance, etc.), error & metric analysis, visualization

of the weights w used for HOPS and HOPS@ k (depicting the impact of proposed weight decay function), and results of FPA computed based on the approach presented by HAFeat. The code for this analysis is provided in *Results and Analysis.ipynb* notebook, which can be used to do this analysis based on the prediction results provided in *out* directory.

Variable	Definition
\mathcal{X}	Dataset
\mathcal{Y}	Set of all class labels $\{y_1, \dots, y_K\}$
\mathcal{T}	Given hierarchy tree corresponding to \mathcal{Y}
H	Height of \mathcal{T}
$\mathcal{V}_{\mathcal{T}}$	Set of all nodes in \mathcal{T}
\mathcal{V}_l	Set of all leaf nodes in \mathcal{T}
n	Total number of nodes in \mathcal{T}
K_l	Number of nodes at level l of \mathcal{T}
K	Number of class labels or leaf nodes in \mathcal{T}
v_i	i -th node in \mathcal{T} , where v_0 is the root
v_{y_i}	Leaf node representing class label y_i
$f_a(v_i)$	Set of all ancestors (excluding root) of a node v_i
$f_d(v_i)$	Set of all descendants of a node v_i
$LCA(y_i, y_j)$	Height of the tree rooted at the Lowest Common Ancestor between leaf nodes y_i and y_j
\mathcal{E}	Set of orthonormal basis vectors $\{e_1, \dots, e_n\}$ that span \mathbb{R}^n
$\mathcal{E}^{(l)}$	Set of basis vectors corresponding to nodes at level l ($\mathcal{E}^{(l)} \subseteq \mathcal{E}$)
\mathcal{E}_i^a	Set of basis vectors corresponding to $f_a(v_i)$ ($\mathcal{E}_i^a \subseteq \mathcal{E}$)
\mathcal{E}_i^d	Set of basis vectors corresponding to $f_d(v_i)$ ($\mathcal{E}_i^d \subseteq \mathcal{E}$)
\mathcal{E}_i	Set of basis vectors defined as $\{\mathcal{E}_i^a \cup \mathcal{E}_i^d\}$
$\neg\mathcal{E}_i$	Set of basis vectors not in \mathcal{E}_i , i.e. $\{\mathcal{E} \setminus \mathcal{E}_i\}$
f_{Θ}	Neural network backbone used as a feature extractor
Z	Vector space containing the feature vectors extracted from f_{Θ}
f_{θ}	Transformation module that transforms the feature vectors from Z
$V_{\mathcal{T}}$	Vector space, defined as $\text{span}(\mathcal{E})$, containing the transformed feature vectors
V_i	Subspace corresponding to a node v_i defined as $\text{span}(\mathcal{E}_i)$
V_i^{\perp}	Complementary subspace to V_i , such that $V_{\mathcal{T}} = V_i + V_i^{\perp}$
\mathbf{z}	Feature vector in Z
\mathbf{x}	Feature vector in $V_{\mathcal{T}}$ defined as $[x_1, \dots, x_n]^{\top}$
\mathbf{x}_{V_i}	Projection of the feature vector onto V_i defined as $\mathbb{P}_{\mathcal{E}_i} \mathbf{x}$
$\mathbb{P}_{\{\dots\}}$	Orthogonal projection operator that computes orthogonal projection of a feature vector onto the vector space spanned by basis vectors $\{\dots\}$
$d_S(\mathbf{x}, V_{y_j})$	Distance of point \mathbf{x} from subspace V_{y_j} , given as $\ \mathbf{x} - \mathbb{P}_{\mathcal{E}_{y_j}} \mathbf{x}\ = \ \mathbb{P}_{\neg\mathcal{E}_{y_j}} \mathbf{x}\ $

Table 8. Notations